



# Geochemistry and tectonic significance of the Gongzhu peridotites in the northern branch of the western Yarlung Zangbo ophiolitic belt, western Tibet

Dongyang Lian<sup>1,2</sup> · Jingsui Yang<sup>1,2</sup> · Fei Liu<sup>1</sup> · Weiwei Wu<sup>1,2</sup> · Li Zhang<sup>1,3</sup> · Hui Zhao<sup>1,3</sup> · Jian Huang<sup>1,3</sup>

Received: 6 April 2016 / Accepted: 1 January 2017 / Published online: 13 January 2017  
© Springer-Verlag Wien 2017

**Abstract** The Gongzhu ophiolite is situated in the northern branch of the western Yarlung Zangbo ophiolitic belt. This massif consists of a strongly dismembered ophiolitic sequence dominated by mantle peridotites. The peridotites comprise lherzolite with low- to moderately-depleted mineral and bulk rock compositions. The degree of partial melting deduced from Cr# values of the Gongzhu peridotites varies between 7% and 10%. The mineral and whole rock compositions of the Gongzhu peridotites are comparable to those of abyssal peridotites. The chondrite normalized REE compositions of the peridotites typically display U-shaped or spoon-shaped patterns, and primitive mantle-normalized PGEs patterns show Ir depletion relative to Os and Ru, and Pt enrichment relative to Rh and Pd. On the basis of the petrological, mineralogical and geochemical data, we concluded that the Gongzhu peridotites either formed in the back-arc setting of an intra-oceanic subduction system or the Gongzhu and Dajiweng peridotites both formed in the same incipient forearc/proto-forearc environment of an intra-oceanic subduction zone.

**Keywords** Yarlung Zangbo ophiolitic belt · Gongzhu ophiolite · Supra-subduction zone · Mantle metasomatism · Subduction initiation

Editorial handling: L. Fedele

✉ Jingsui Yang  
yangj sui@163.com

<sup>1</sup> Center for Advanced Research on Mantle (CARMA), Institute of Geology, Chinese Academy of Geological Sciences, Beijing 100037, China

<sup>2</sup> Faculty of Earth Sciences, China University of Geosciences (Wuhan), Wuhan 430074, China

## Introduction

Ophiolites represent remnants of ancient oceanic crust and upper mantle that were obducted on to the continental margin or other buoyant tract due to tectonic collision or underplating events (Pearce et al. 1984; Wakabayashi et al. 2010; Whattam and Stern 2011; Dilek and Furnes 2014; Pearce 2014). An intact ophiolite consists of (from bottom to top) residual mantle, magmatic crust and sedimentary cover (Penrose 1972; Dilek and Furnes 2011; Whattam and Stern 2011). However, most ophiolites are incomplete and highly dismembered and/or tectonized (Whattam and Stern 2011). Ophiolites preserve valuable information for understanding the evolution and geodynamic processes of ancient oceans.

Mantle peridotites in ophiolites are interpreted as the result of a series of mantle processes including partial melting, melt extraction and melt-mantle interaction (Parkinson and Pearce 1998; Bizimis et al. 2000; Pearce et al. 2000; Takazawa et al. 2000; Niu 2004; Krishnakanta Singh 2013). The chemical composition data of these rocks and their constituent minerals preserve important information on these mantle processes, which can be used to constrain the tectonic evolution of ophiolites. In peridotites, light rare earth elements (LREE) are incompatible during partial melting (Pearce et al. 1984; Parkinson and Pearce 1998; Pearce et al. 2000; Niu 2004). As so, mantle peridotites become progressively more depleted in LREE with increased melting. However, melt-rock reaction after mantle melting may result in U-shaped or spoon-shaped REE patterns, which have been reported from ophiolites worldwide (Parkinson and Pearce 1998; Pearce et al. 2000; Melcher et al. 2002; Bezard et al. 2011; Uysal et al. 2012; Saka et al. 2014).

On the basis of varying chemical behaviors and different melting temperatures, Platinum Group Elements (PGE) can be divided into an iridium group (IPGE: Os, Ir, and Ru) and a

palladium group elements (PPGE: Rh, Pt and Pd) (Barnes 1993; Barnes and Picard 1993; Lorand et al. 1999; Jannessary et al. 2012). IPGEs have melting temperatures  $>2000$  °C and behave as compatible elements during mantle melting, whereas PPGE have melting temperatures  $<2000$  °C and act as incompatible elements (Woodland et al. 2002). Thus, partial melting can effectively fractionate IPGE from PPGE and hence will generally decrease Pd/Ir ratios in melting residues as the degree of melting increases (Alard et al. 2000; Jannessary et al. 2012; Osbahr et al. 2014). As with LREE, PPGE enrichment in mantle peridotites may also result from melt-rock reaction.

Peridotites from ophiolites within the Yarlung Zangbo Suture Zone (YZSZ) have been widely studied (Dubois-Cote et al. 2005; Bédard et al. 2009; Liu et al. 2010; Bezahl et al. 2011; Dai et al. 2011; Xu et al. 2011; Niu et al. 2015). However, studies on ophiolites from the northern branch of the western YZSZ are scarce.

Here, we present our study of peridotite samples from the Gongzhu ophiolite in the northern branch of the western

Yarlung Zangbo Suture Zone (YZSZ) ophiolitic belt. We describe and interpret mineral and bulk rock geochemistry in order to reconstruct the tectonic, magmatic, and metasomatic history of the Gongzhu ophiolite. The Dajiweng ophiolite also lies in the northern branch of the western YZSZ ophiolitic belt. As the Dajiweng peridotites are interpreted as having formed in a forearc environment (Lian et al. 2016), data of the Dajiweng peridotite are cited in this paper to facilitate a comparison with the Gongzhu peridotites.

## Geological background

The Tibetan plateau consists of several terranes, which were once separated by the Paleo- and Neo-Tethyan Oceans (Nicolas et al. 1981; Tapponnier et al. 1981; Yin and Harrison 2000; Xu et al. 2012; Zhu et al. 2013). The final closure of the Paleo- and Neo-Tethyan Oceans generated four main sutures. From north to south these are: A'nmagin-Kunlun, Jinshajiang, Bangong-Nujiang and Yarlung Zangbo (Tapponnier et al. 1981; Burg

**Fig. 1** **a** Overview map of the India-Eurasia collision zone, showing the location of the study area (red box). **b** Distribution of the ophiolites along the Yarlung Zangbo suture zone (YZSZ) and Bangong Nujiang Suture Zone (BNSZ) in Tibet. ES: Eastern Segment, CS: Central Segment, WS: Western Segment of the YZSZ. **c** Simplified geological map of the western segment of the YZSZ. Modified from Liu et al. (2015a).

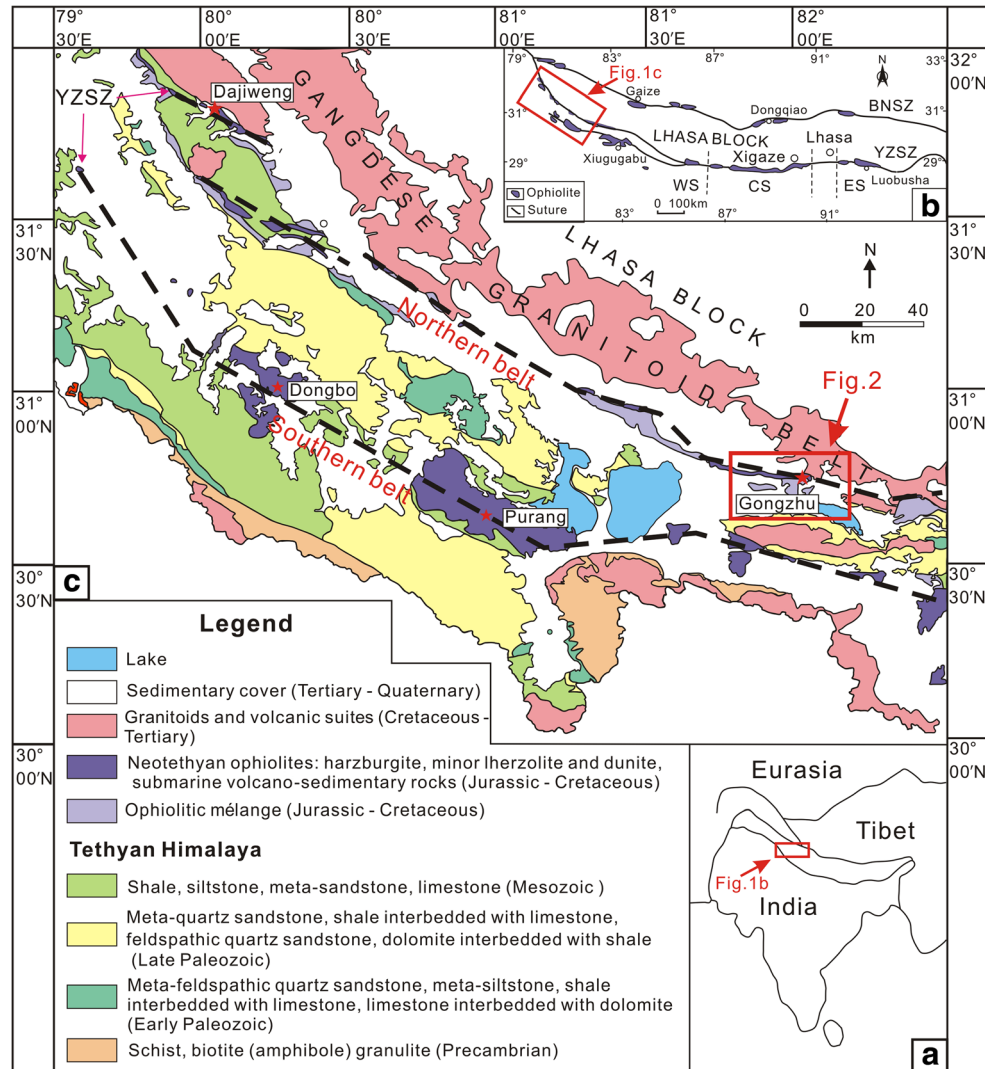
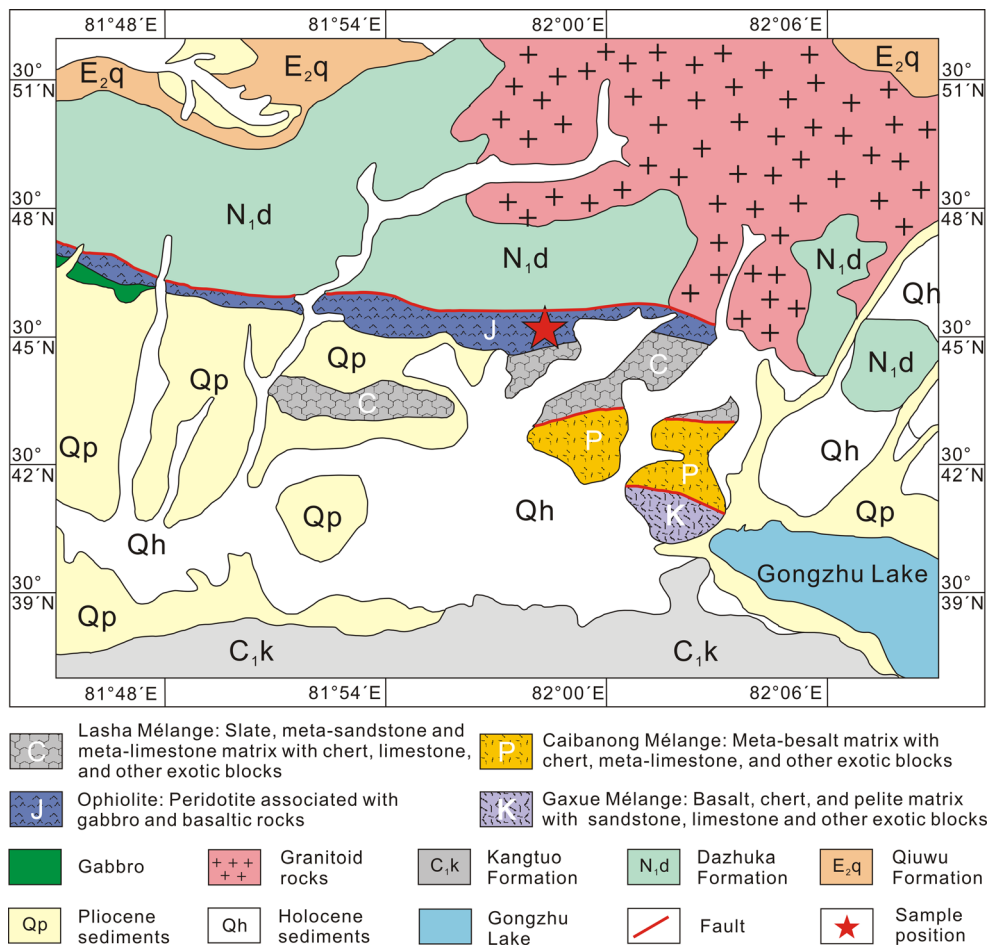


**Fig. 2** Simplified geological map of the Gongzhu ophiolite



and Chen 1984; Girardeau et al. 1985; Yin and Harrison 2000; Xu et al. 2012). The E-W trending Yarlung Zangbo suture, which

extends over more than 2000 km in southern Tibet, is the youngest and southernmost of the four (Liang et al. 2014; Xiong et al.

**Fig. 3** Field photographs of the Gongzhu ophiolite. **a** The Gongzhu peridotites in the field; **b** Strongly serpentinized Gongzhu peridotite; **c** Block of gabbro in contact with peridotites of the Gongzhu ophiolite; **d** Strongly deformed cherts in the Gongzhu ophiolite

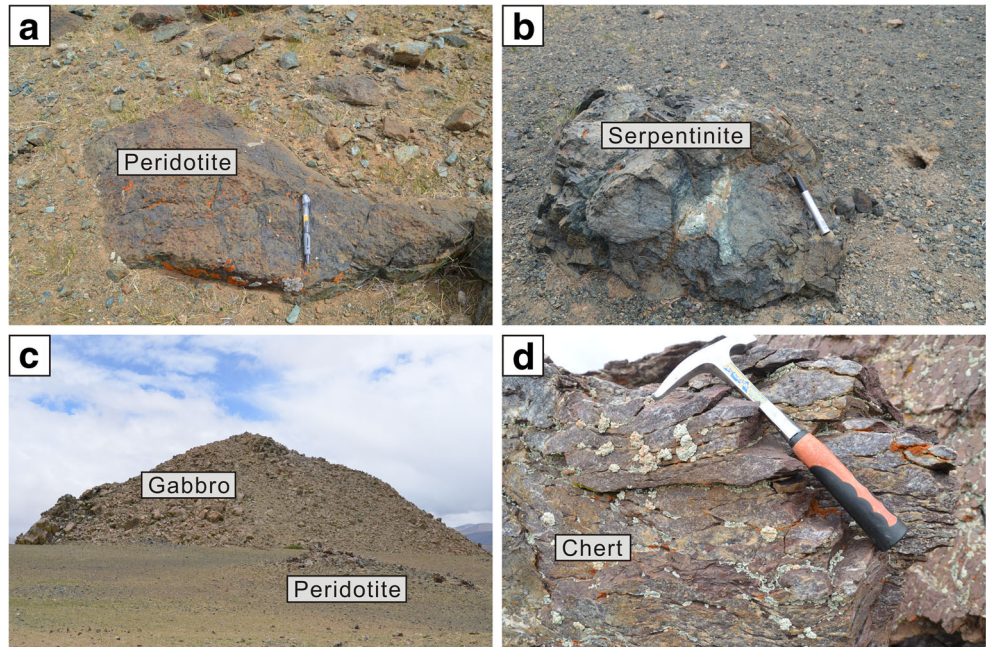
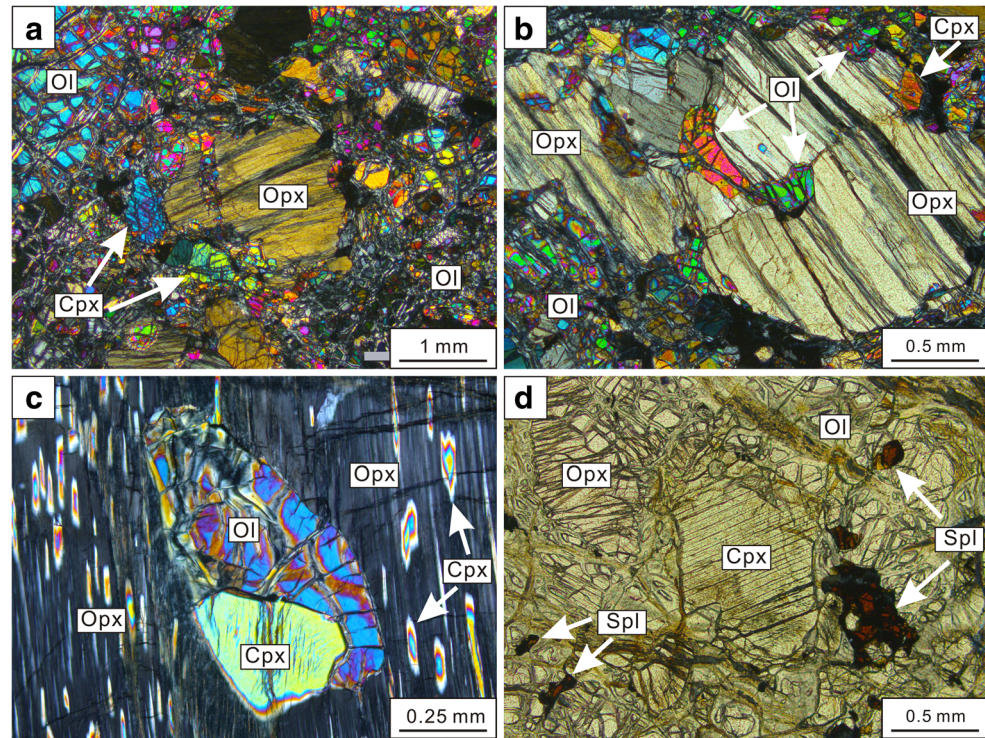


**Fig. 4** Photomicrographs of peridotites from the Gongzhu ophiolite. **a** Gongzhu lherzolite showing mineral distribution; **b** Interstitial olivine occurring in the embayment of orthopyroxene; **c** Olivine and clinopyroxene as inclusions in orthopyroxene; **d** Spinel in Gongzhu peridotite. Ol—olivine; Opx-orthopyroxene; Cpx-clinopyroxene; Spl-spinel



2015; Xu et al. 2015). The YZSZ is composed of four major lithotectonic units, from north to south: the Gangdese magmatic arc, Xigaze forearc basin, Yarlung Zangbo ophiolitic belt and a Triassic-Eocene accretionary wedge (Ding et al. 2005; Wang et al. 2012). However, the tectonic configurations of the YZSZ vary spatially from the east to the west. The Xigaze forearc basin sequence is well developed in the central segment of YZSZ

(from Renbu to Saga), however this unit is absent in the eastern (from Renbu to the east) and western segment (from Saga to the west) Xu et al. (2011); Wang et al. 2012).

Ophiolites distributed along YZSZ represent remnants of the Neo-Tethyan Ocean that once separated the Lhasa block from the Indian plate (Nicolas et al. 1981; Tapponnier et al. 1981; Burg and Chen 1984; Girardeau et al. 1985). Ophiolites

**Table 1** Representative microprobe analyses of olivine in the Gongzhu peridotites

Lithology	Analyzing No.	SiO <sub>2</sub>	TiO <sub>2</sub>	Al <sub>2</sub> O <sub>3</sub>	Cr <sub>2</sub> O <sub>3</sub>	FeO <sup>t</sup>	MnO	MgO	NiO	CaO	K <sub>2</sub> O	Na <sub>2</sub> O	Total	Fo
Gongzhu peridotite	14YP-12-4-7	40.91	b.d.	0.03	0.02	9.57	0.17	49.12	0.34	b.d.	0.02	b.d.	100.18	90.0
	14YP-12-4-11	41.19	0.01	0.01	0.07	8.80	0.13	48.57	0.46	b.d.	0.02	0.01	99.25	90.7
	14YP-12-5-4	41.20	b.d.	b.d.	0.01	9.16	0.16	48.36	0.46	b.d.	0.01	b.d.	99.35	90.3
	14YP-12-5-5	41.14	b.d.	b.d.	0.04	9.14	0.13	48.80	0.40	b.d.	0.01	0.01	99.68	90.4
	14YP-13-4-2	41.12	b.d.	b.d.	0.03	9.40	0.14	48.59	0.38	b.d.	b.d.	0.01	99.68	90.1
	14YP-13-4-5	41.18	0.05	0.02	0.06	9.31	0.12	48.89	0.47	0.01	b.d.	0.01	100.12	90.2
	14YP-13-6-1	41.07	b.d.	b.d.	0.01	9.12	0.14	48.41	0.46	0.01	0.01	b.d.	99.23	90.3
	14YP-13-6-15	40.70	0.01	0.02	b.d.	10.16	0.10	48.65	0.43	b.d.	b.d.	0.01	100.08	89.4
	14YP-12-6-12	40.99	b.d.	0.00	b.d.	9.31	0.13	48.68	0.39	b.d.	b.d.	b.d.	99.49	90.2
	14YP-12-6-15	41.52	b.d.	b.d.	b.d.	8.52	0.08	49.24	0.43	b.d.	b.d.	b.d.	99.80	91.0
	14YP-12-7-1	41.62	0.02	0.01	b.d.	9.04	0.11	48.79	0.43	b.d.	b.d.	b.d.	100.01	90.5
	14YP-12-7-13	41.10	0.02	b.d.	b.d.	9.05	0.12	49.33	0.36	b.d.	b.d.	b.d.	99.98	90.6
	14YP-12-8-12	41.14	0.03	b.d.	b.d.	8.59	0.12	49.15	0.39	0.01	b.d.	b.d.	99.43	91.0
	14YP-12-8-14	41.20	b.d.	0.02	b.d.	8.88	0.14	48.94	0.39	0.01	b.d.	b.d.	99.58	90.6
	14YP-12-9-10	41.95	0.02	b.d.	0.03	9.18	0.11	48.25	0.42	b.d.	b.d.	0.03	100.00	90.3
	14YP-12-9-15	41.69	b.d.	b.d.	b.d.	8.54	0.13	48.66	0.35	b.d.	0.02	0.01	99.40	90.9

b.d. = below detection limit, FeO<sup>t</sup> = total iron oxide

along the YZSZ include the Zedang and Luobusa ophiolite in the eastern segment, and the Xigaze, Jiding and Sangsang ophiolites in the central segment. From the Saga to the west, the YZSZ ophiolitic belt divides into two branches: the southern branch and the northern branch (Fig. 1). The northern branch comprises the Gongzhu, Baer, and Dajiweng massifs, while the southern branch includes the Saga, Zhongba, Xiugugabu, Purang and Dongbo massifs (Liu et al. 2010; Bezahl et al. 2011; Dai et al. 2011; Xiong et al. 2013; Liu et al. 2015a; Xu et al. 2015). The Dajiweng massif is situated in the westernmost part of the northern branch, consisting mainly of harzburgites with minor volcanic rocks and cherts (Lian et al. 2016). High-Cr chromitites with massive, disseminated or nodular textures can be observed in the Dajiweng harzburgites. A dunite shell commonly exists between the chromitites and the harzburgites.

The Gongzhu ophiolite, one of the main segments of the northern branch, is located about 15 km southwest of the Gongzhu Lake in the northern branch of the western YZSZ ophiolitic belt, southwestern Tibet (Fig. 2). The Gongzhu massif is bounded by Gangdese granitic rocks and the Dazhuka formation in the north, and covered by Quaternary sediments in the south. The Dazhuka formation is mainly composed of Paleocene conglomerate and sandstone. The Gongzhu ophiolite exhibits a relatively intact sequence, which includes peridotites, gabbro, volcanic rocks and cherts. The mantle sequence of this ophiolite is dominated by lherzolites and serpentinites. No dykes or podiform chromitites were found in the Gongzhu peridotites.

## Petrography

The Gongzhu massif mainly comprises ultramafic rocks, gabbro, volcanic rocks and cherts (Fig. 3). The ultramafic rocks are dominated by lherzolites (6%–7% modal clinopyroxene). All of the peridotites show various degree of serpentinization and some of these peridotites are completely serpentinized (Fig. 3b). The relatively fresh peridotite samples were chosen for petrological and mineralogical study.

Lherzolites from the Gongzhu massif mainly show porphyroclastic texture. Olivines are the most abundant minerals in the lherzolites. The modal volume contents of olivine range from 65% to 70%. Olivines in the Gongzhu peridotite generally have two textural types: as millimeter-size porphyroclasts (Fig. 4a) and as anhedral fine-grained crystals (Fig. 4b). Olivine porphyroclasts often show wavy extinction or kink bands indicating internal deformation. Fine-grained olivines either occur in the embayment of orthopyroxene porphyroclasts or as inclusions in orthopyroxene and

spinel (Fig. 4b, c). No olivine grains have been observed to be enclosed in clinopyroxene.

Orthopyroxene in the Gongzhu peridotites makes up 25%–30% volume of the modal mineralogy. Orthopyroxene appears either as porphyroclasts (1–2 mm) with clinopyroxene exsolution lamellae (Fig. 4c), or as interstitial irregular fine-grained neoblasts (0.1–0.5 mm). Rounded olivine and clinopyroxene inclusions can occasionally be observed in orthopyroxene porphyroclasts (Fig. 4c).

The modal volume of clinopyroxene varies between 6% and 7%. Clinopyroxene also has various occurrences, including as: 1) interstitial subhedral or anhedral grains (0.2–0.7 mm) (Fig. 4a), 2) subhedral porphyroclasts (1–1.5 mm) (Fig. 4d), 3) irregular-shaped inclusions in

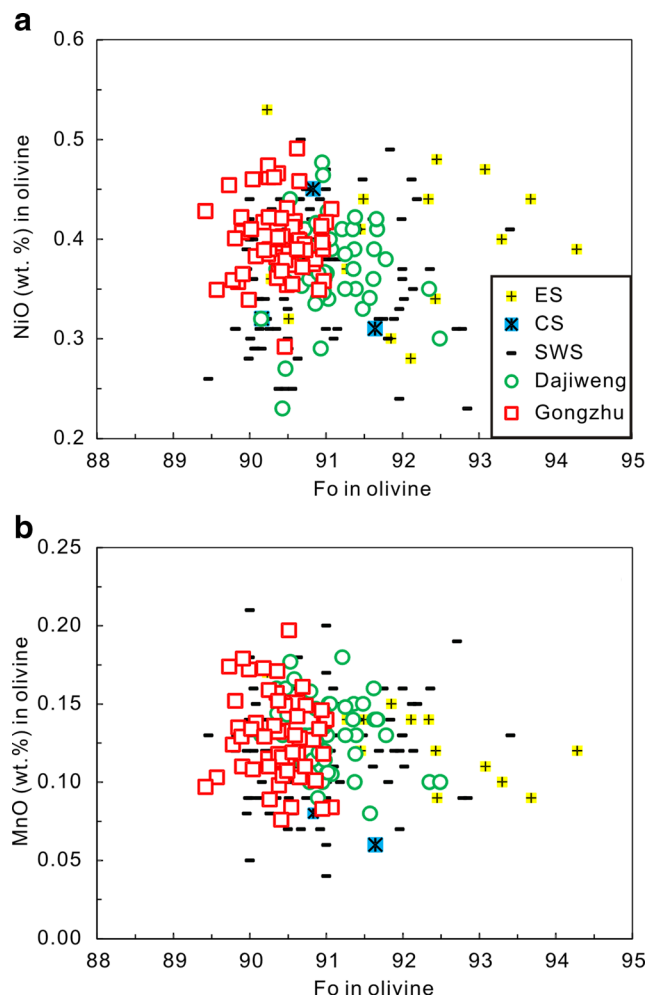
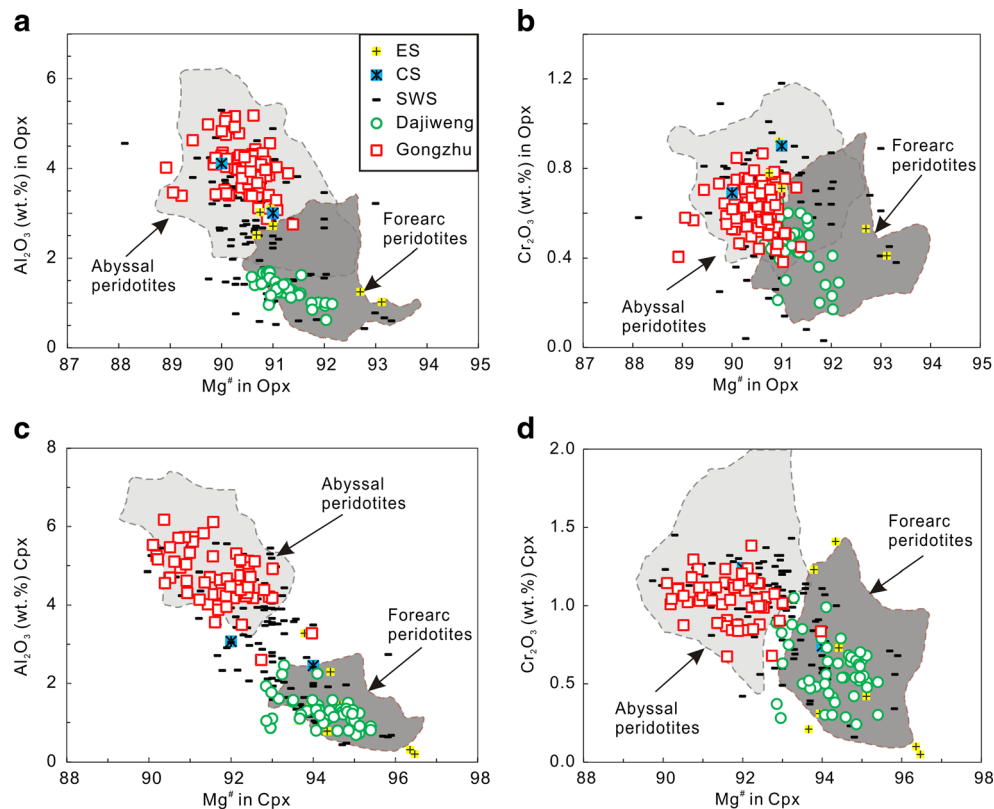


**Fig. 5** Compositional variations of olivines in peridotites from the YZSZ. **a** NiO vs. forsterite (Fo) and **b** MnO vs. Fo. DJW-Dajiweng peridotite. The eastern segment (ES) includes the Luobusa and Kangjinla ophiolite (Malpas et al. 2003; Xu et al. 2011). The central segment (CS) includes the Xigaze and Sangsang ophiolite (Bédard et al. 2009). The southern branch of western segment (SWS) includes the Saga (Bédard et al. 2009), Zhongba (Dai et al. 2011), Xiugugabu (Bezahl et al. 2011), Purang (also called Yungbwa or Jungbwa) (Liu et al. 2010) and Dongbo (also called Kiogar) ophiolites (Niu et al. 2015)

**Fig. 6** Compositional variations of orthopyroxene and clinopyroxene in peridotites from the YZSZ. **a**  $\text{Al}_2\text{O}_3$  vs. Mg# for Opx; **b**  $\text{Cr}_2\text{O}_3$  vs. Mg# for Opx; **c**  $\text{Al}_2\text{O}_3$  vs. Mg# for Cpx; and **d**  $\text{Cr}_2\text{O}_3$  vs. Mg# for Cpx. Fields of forearc and abyssal peridotites are from Lian et al. (2016)



orthopyroxene (Fig. 4c), and 4) small exsolution lamellae in orthopyroxene (Fig. 4c).

Spinel in the harzburgite are generally reddish brown with modal volume contents of 1%–2% (Fig. 4d). They are anhedral and range from 0.1 mm

to 0.5 mm in size. Olivine or orthopyroxene inclusions can occasionally be found in spinel.

Secondary minerals including serpentine and magnetite are very common along the fissures and cracks of the aforementioned silicate minerals (Fig. 4d).

**Table 2** Representative microprobe analyses of orthopyroxene in the Gongzhu peridotites

Lithology	Analyzing No.	$\text{SiO}_2$	$\text{TiO}_2$	$\text{Al}_2\text{O}_3$	$\text{Cr}_2\text{O}_3$	$\text{FeO}^t$	$\text{MnO}$	$\text{MgO}$	$\text{CaO}$	$\text{Na}_2\text{O}$	$\text{K}_2\text{O}$	$\text{NiO}$	Total	$\text{Wo}$	$\text{En}$	$\text{Fs}$	Mg#
Gongzhu peridotite	14YP-12-4-1	55.15	0.04	4.35	0.70	6.33	0.13	31.78	1.12	0.02	b.d.	0.05	99.69	2.2	87.7	10.0	90.0
	14YP-12-4-4	54.59	0.08	4.09	0.61	6.05	0.13	30.90	2.47	0.06	0.02	0.13	99.13	4.9	85.3	9.6	90.2
	14YP-12-5-2	55.23	0.11	3.96	0.54	6.23	0.14	32.25	0.86	b.d.	b.d.	0.13	99.44	1.7	88.5	9.8	90.3
	14YP-12-5-6	55.57	0.09	3.57	0.50	6.20	0.19	32.48	0.67	0.03	b.d.	0.08	99.39	1.3	88.7	9.8	90.4
	14YP-13-4-3	55.08	0.03	4.24	0.65	6.18	0.13	32.10	0.58	0.04	b.d.	0.08	99.10	1.2	88.9	9.8	90.3
	14YP-13-4-7	55.05	0.07	4.22	0.58	6.23	0.18	31.57	1.03	b.d.	b.d.	0.10	99.02	2.1	87.9	10.1	90.1
	14YP-13-6-2	53.95	0.06	3.39	0.57	7.18	0.13	33.10	0.49	0.05	0.04	0.10	99.06	0.9	88.1	10.8	89.2
	14YP-13-6-4	55.50	0.01	3.93	0.70	6.22	0.14	32.59	0.73	b.d.	0.01	0.05	99.87	1.4	88.8	9.7	90.4
	14YP-12-6-3	55.51	0.09	4.00	0.67	5.91	0.15	32.45	0.79	0.03	0.01	0.07	99.68	1.6	89.0	9.4	90.8
	14YP-12-6-7	55.57	0.12	4.25	0.79	6.02	0.11	31.72	1.17	0.03	b.d.	0.06	99.84	2.3	88.0	9.6	90.5
	14YP-12-7-2	55.94	0.05	3.76	0.63	5.95	0.14	31.62	1.53	0.05	b.d.	0.12	99.79	3.0	87.3	9.5	90.5
	14YP-12-7-6	56.22	0.01	3.29	0.51	5.80	0.18	32.90	0.77	0.04	b.d.	0.07	99.80	1.5	89.2	9.1	91.1
	14YP-12-8-5	55.29	0.07	3.81	0.63	6.01	0.12	32.84	0.86	b.d.	b.d.	0.09	99.73	1.7	89.0	9.3	90.7
	14YP-12-8-8	54.91	0.05	3.93	0.69	6.07	0.16	32.43	0.88	0.03	b.d.	0.08	99.22	1.7	88.6	9.6	90.6
	14YP-12-9-11	56.14	0.03	3.97	0.78	5.82	0.13	32.19	0.74	0.00	b.d.	0.11	99.92	1.5	89.2	9.3	90.9
	14YP-12-9-16	56.10	0.02	3.68	0.58	5.95	0.16	32.30	0.68	0.02	0.02	0.07	99.56	1.4	89.1	9.5	90.7

b.d. = below detection limit,  $\text{FeO}^t$  = total iron oxide,  $\text{Mg}\# = 100 * \text{Mg}/(\text{Mg} + \text{Fe}^{2+})$ ,  $\text{Fe}^{2+}$  is total iron

## Analytical methods

Peridotites with relatively low degrees of serpentinization and alteration were analyzed for their whole rock and mineral geochemistry. Mineral analyses were performed with a JEOL JXA-8100 electron microprobe at the State Key Laboratory of Continental Tectonics and Dynamics, Institute of Geology, Chinese Academy of Geological Sciences. Measurements were performed at 15 kV and 20 nA, with a counting time of 10 s on peak and 5 s for background, using a beam in fix mode, and 5 μm size.

Bulk rock major oxides and trace elements were analyzed at the National Research Center for Geoanalysis in Beijing, China. All samples were carefully cleaned, crushed and then ground in an agate mortar to pass a 200-mesh screen. Major oxides of sample 14YP-13-6 were measured twice. Major elements were determined by X-ray fluorescence on fused glass beads using PW4400 spectrometry. Trace elements, including the REE, were determined by inductively coupled mass spectrometry (ICP-MS). One national standard sample (GBW07105) (Klemm and Bombach 2001) was measured simultaneously to ensure consistency of the analytical results. These results indicate that the accuracy is better than 10% for most elements, with many elements better than 5% of the recommended values (Table 5). Platinum group elements were analyzed at the National Research Center for Geoanalysis, Chinese Academy of Geological Sciences, Beijing. Detailed analytical processes for the platinum group elements have been described by Xiong et al. (2013). Water and CO<sub>2</sub> were determined by gravimetric techniques in which a sample is heated in a closed container and the water vapor is

collected in a separate tube, condensed and then weighed. The detection limit for H<sub>2</sub>O and CO<sub>2</sub> is 0.01 wt.%.

## Mineral chemistry

Representative compositions of olivine from the Gongzhu Iherzolites are listed in Table 1. These olivines have Fo contents ranging from 89.4 to 91.1. No correlation can be observed between Fo and NiO or Fo and MnO contents (Fig. 5a, b). Orthopyroxenes in the Gongzhu Iherzolites have an average composition of En<sub>88</sub>Fs<sub>10</sub>Wo<sub>2</sub>. On the Opx diagrams (Fig. 6a, b), orthopyroxenes have Al<sub>2</sub>O<sub>3</sub> (2.75–5.76 wt.%) and Cr<sub>2</sub>O<sub>3</sub> (0.38–0.85 wt.%) contents correlating with Mg# values (89.1–93.0). TiO<sub>2</sub> contents of orthopyroxene vary between 0.01 wt.% and 0.13 wt.% (Table 2). Representative electron microprobe analyses of clinopyroxene are listed in Table 3. Clinopyroxenes have an average composition of En<sub>47</sub>Fs<sub>5</sub>Wo<sub>48</sub> with Mg# values ranging from 88.4 to 93.0 (Table 3). Al<sub>2</sub>O<sub>3</sub> (2.60–6.17 wt.%) and Cr<sub>2</sub>O<sub>3</sub> (0.68–1.38 wt.%) contents also inversely correlate with Mg# in clinopyroxene (Fig. 6c, d). Spinels have Cr# values ranging from 18.3 to 25.7 and Mg# values varying between 87.6 and 78.8 (Fig. 7a, b) (Table 4). Spinels are also characterized by low TiO<sub>2</sub> and high NiO concentrations.

## Bulk-rock geochemistry

Bulk-rock geochemistry analyses for the Gongzhu Iherzolites are listed in Table 5. The Gongzhu Iherzolite has experienced variable degrees of serpentinization with LOI of 6.8–9.1 wt.% (Table 5). Al<sub>2</sub>O<sub>3</sub>/SiO<sub>2</sub> and

**Table 3** Representative microprobe analyses of clinopyroxene in the Gongzhu peridotites

Lithology	Analyzing No.	SiO <sub>2</sub>	TiO <sub>2</sub>	Al <sub>2</sub> O <sub>3</sub>	Cr <sub>2</sub> O <sub>3</sub>	FeO <sup>t</sup>	MnO	MgO	CaO	Na <sub>2</sub> O	K <sub>2</sub> O	NiO	Total	Wo	En	Fs	Mg#
Gongzhu peridotite	14YP-12-4-2	50.86	0.12	5.10	1.16	2.31	0.08	15.35	23.75	0.32	0.01	0.04	99.10	49.9	44.9	3.9	92.3
	14YP-12-4-3	51.74	0.14	5.12	1.04	2.35	0.12	15.94	22.39	0.37	0.01	0.04	99.26	47.5	47.0	4.1	92.4
	14YP-12-5-3	51.18	0.22	4.96	1.29	2.80	0.11	15.29	23.64	0.53	b.d.	0.01	100.01	49.1	44.2	4.7	90.8
	14YP-12-5-7	51.44	0.27	4.02	0.89	2.69	0.17	16.02	23.36	0.43	b.d.	0.02	99.31	48.0	45.8	4.6	91.4
	14YP-13-4-4	51.59	0.15	4.27	0.87	2.71	0.12	16.40	23.56	0.27	0.01	0.08	100.03	48.0	46.5	4.5	91.6
	14YP-13-4-6	50.94	0.17	4.58	0.89	2.68	0.13	15.79	23.87	0.34	b.d.	0.06	99.44	49.1	45.2	4.5	91.4
	14YP-13-6-3	51.38	0.15	3.88	1.04	2.64	0.10	16.19	24.29	0.28	0.01	0.02	99.99	49.1	45.6	4.3	91.7
	14YP-13-6-5	52.82	0.10	3.50	0.85	2.44	0.07	16.22	22.93	0.29	b.d.	0.10	99.31	47.8	47.0	4.1	92.3
	14YP-12-6-4	52.90	0.28	4.22	1.05	2.38	0.07	16.01	22.48	0.47	0.02	0.05	99.93	47.3	46.9	4.0	92.4
	14YP-12-6-11	52.74	0.24	4.23	0.88	2.56	0.09	16.13	22.01	0.37	0.03	0.06	99.34	46.6	47.6	4.4	91.9
	14YP-12-7-10	53.00	0.13	4.31	1.15	2.39	0.07	16.14	21.65	0.53	b.d.	0.05	99.42	46.1	47.8	4.1	92.4
	14YP-12-7-16	53.21	0.14	3.96	0.84	2.53	0.08	15.97	23.27	0.46	b.d.	0.04	100.51	48.1	45.9	4.2	91.9
	14YP-12-8-10	52.29	0.13	4.21	0.90	2.15	0.11	15.73	23.77	0.50	0.02	0.01	99.82	49.2	45.3	3.7	92.9
	14YP-12-8-3	52.32	0.22	4.18	1.02	2.11	0.06	15.62	24.38	0.50	b.d.	0.05	100.45	50.1	44.6	3.5	93.0
	14YP-12-9-12	52.47	0.09	5.14	1.38	2.30	0.10	15.19	22.08	0.63	b.d.	0.06	99.45	47.8	45.7	4.1	92.2
	14YP-12-9-17	53.14	0.11	4.47	1.21	2.42	0.09	15.48	21.96	0.56	0.01	0.06	99.50	47.3	46.3	4.3	92.0

b.d. = below detection limit, FeO<sup>t</sup> = total iron oxide, Mg# = 100\*Mg/(Mg + Fe<sup>2+</sup>), Fe<sup>2+</sup> is total iron

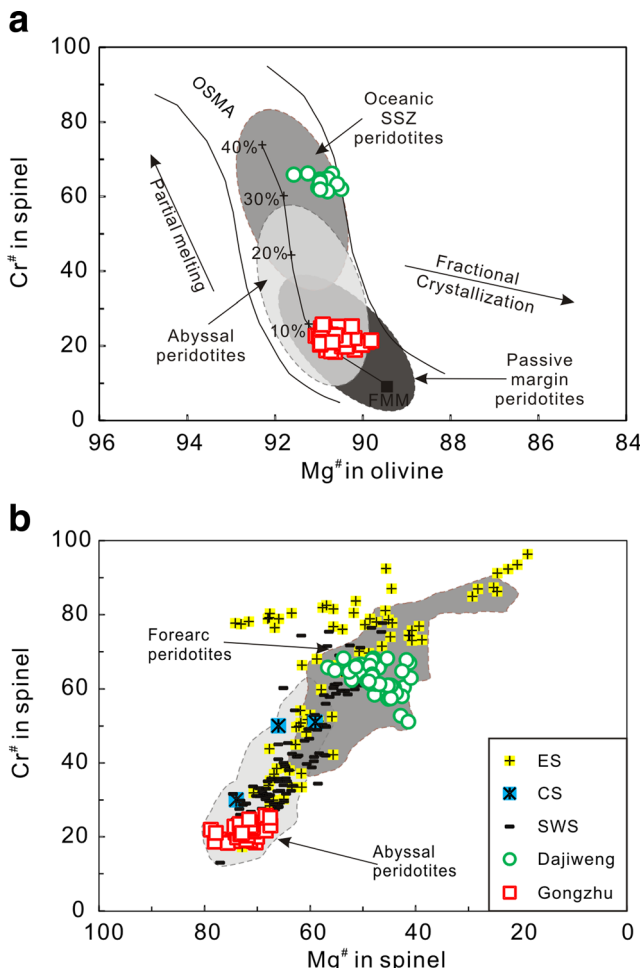


**Fig. 7** Compositional variations of spinel in peridotites from the YZSZ. **a** Spinel Cr# against olivine Fo value after Pearce et al. (2000); **b** Cr# vs. Mg# of spinel. OSMA-Olivine-spinel mantle array; FMM-Fertile MORB mantle; SSZ-suprasubduction zone. Spinel composition data of abyssal and forearc peridotites are from the same references as pyroxenes in Fig. 6

MgO/SiO<sub>2</sub> ratios are 0.03–0.04 and 0.88–0.98 respectively, which is within the field of abyssal peridotites (Fig. 8). The major oxide contents are normalized on anhydrous basis. Peridotites have Mg# [100\*Mg<sup>2+</sup> / (Mg<sup>2+</sup> + Fe<sup>2+</sup>)] of 93–94, with Al<sub>2</sub>O<sub>3</sub> and CaO contents of 1.36–1.98 wt.% and 1.40–2.05 wt.%, respectively (Fig. 9). The chondrite normalized REE compositions of the peridotites typically display U-shaped or spoon-shaped patterns, with (La/Sm)<sub>N</sub> ranging between 1.0 and 5.9 (Fig. 10a). In the primitive mantle-normalized trace element spider diagrams, the Gongzhu peridotites show prominent positive U anomalies, with slightly negative Sr, Zr and Eu anomalies (Fig. 10b). Total platinum group element contents ( $\Sigma$ PGE) of the Gongzhu peridotites range from 17.3 to 24.3 ppb. Primitive mantle-normalized PGEs patterns show Ir depletion relative to Os and Ru, and Pt enrichment relative to Rh and Pd (Fig. 11).

## Discussion

### Nature of partial melting

Important information of mantle melting history can be preserved by the modal mineralogy, mineral chemistry and whole-rock chemical compositions. Clinopyroxene is generally considered to be the most rapidly consumed mineral during partial melting (Jaques and Green 1980; Baker and Stolper 1994; Parkinson and Pearce 1998). The modal volume proportion of clinopyroxene in peridotite is estimated to be in the range from 15% in fertile peridotite (with 0% partial melting) to 0% in depleted peridotite (after 25% partial melting) (Parkinson and Pearce 1998). The Gongzhu peridotites have clinopyroxene contents of 6–8% suggesting a moderate degree of partial melting. Pyroxenes from the Gongzhu peridotites have lower Mg# values but higher Al<sub>2</sub>O<sub>3</sub> and Cr<sub>2</sub>O<sub>3</sub> contents than those of the Dajiweng peridotites, indicating that the Gongzhu peridotites experienced a lower degree of partial melting (Fig. 6).

Forsterite contents of olivine and Cr# values of spinel in peridotite are useful indicators of degree of melting (Dick and Bullen 1984; Arai 1994). Olivines in the Gongzhu peridotite have relatively lower Fo contents than those of the Dajiweng harzburgite indicating a lower degree of partial melting (Fig. 5). MnO and NiO contents in olivine show no significant correlation with Fo contents. In the plot of Cr# in spinel versus Mg# in olivine, all of the Gongzhu peridotites plot in the olivine-spinel mantle array (OSMA) (Fig. 7a), indicating that the Gongzhu peridotites are residual after a relatively low degree of partial melting (6%–10%) (Arai 1994). According to the equation proposed by Hellebrand et al. (2001), the partial melting degree of the Gongzhu peridotite can be quantitatively determined by Cr# values of spinel. Based on the Cr# values, the Gongzhu peridotites have experienced 7%–10% degree of partial melting (Hellebrand et al. 2001).

In the plot of MgO/SiO<sub>2</sub> versus Al<sub>2</sub>O<sub>3</sub>/SiO<sub>2</sub> (Fig. 8) (Jagoutz et al. 1979), Gongzhu peridotites plot below (but very close to), the melting trend, reflecting a relatively low effect of secondary alteration or serpentinization processes on the major oxide composition (Snow and Dick 1995). For this reason the whole rock geochemical data of the Gongzhu peridotite can be considered pristine and used to evaluate the melting process. Higher Al<sub>2</sub>O<sub>3</sub>, CaO, SiO<sub>2</sub> contents, but lower MgO and Ni contents of the Gongzhu peridotites compared to those of the Dajiweng harzburgites are attributed to lower degrees of partial melting (Fig. 9). Rare earth elements (REE) are incompatible during partial melting and with higher degree of partial melting, the REE content will become lower in the melting residues. As HREE are unsusceptible to mantle metasomatism, they can also help to constrain the depletion degree of the mantle peridotites (Fig. 10a, b) (Pearce and Parkinson 1993). In Fig. 10a, based on the melting model by

**Table 4** Representative microprobe analyses of spinel in the Gongzhu peridotites

Lithology	Analyzing No.	$\text{Cr}_2\text{O}_3$	$\text{Al}_2\text{O}_3$	$\text{TiO}_2$	$\text{FeO}^t$	MgO	MnO	NiO	CaO	$\text{K}_2\text{O}$	$\text{Na}_2\text{O}$	$\text{SiO}_2$	Total	Mg#	Cr#
Gongzhu peridotite	14YP-12-4-12	17.47	50.45	b.d.	13.47	17.38	0.20	0.25	b.d.	b.d.	b.d.	0.05	99.27	70.7	18.8
	14YP-12-4-17	18.68	49.54	b.d.	12.63	18.17	0.17	0.32	b.d.	b.d.	0.04	0.04	99.61	73.8	20.2
	14YP-12-5-1	21.63	46.16	0.03	13.71	17.06	0.19	0.20	0.02	b.d.	0.03	0.02	99.03	70.6	23.9
	14YP-12-5-9	19.07	47.86	0.07	14.08	18.26	0.17	0.28	0.02	0.02	0.01	0.04	99.87	74.1	21.1
	14YP-13-4-1	18.81	48.98	0.05	12.97	18.09	0.17	0.26	b.d.	0.02	b.d.	0.01	99.36	73.5	20.5
	14YP-13-4-10	19.23	49.47	0.03	12.83	17.93	0.15	0.28	b.d.	b.d.	0.01	0.01	99.95	72.6	20.7
	14YP-13-6-6	19.32	48.52	0.03	11.93	19.28	0.14	0.31	0.01	b.d.	0.02	0.02	99.57	77.8	21.1
	14YP-13-6-7	20.77	48.00	0.02	12.21	18.04	0.14	0.28	b.d.	b.d.	0.02	0.01	99.49	73.6	22.5
	14YP-12-6-13	20.40	46.40	0.08	13.61	18.11	0.17	0.27	b.d.	b.d.	0.02	0.13	99.18	74.3	22.8
	14YP-12-6-5	19.17	46.44	0.04	16.53	16.55	0.16	0.19	b.d.	0.01	0.02	0.01	99.10	68.4	21.7
	14YP-12-7-11	20.72	46.10	b.d.	14.48	17.22	0.15	0.28	0.01	0.01	0.02	0.04	99.02	71.3	23.2
	14YP-12-7-12	22.13	44.19	0.05	16.42	16.35	0.17	0.23	b.d.	b.d.	b.d.	0.01	99.56	68.0	25.1
	14YP-12-8-1	20.23	46.52	0.04	15.01	17.23	0.17	0.23	b.d.	0.01	b.d.	0.01	99.45	70.8	22.6
	14YP-12-8-11	18.83	48.51	0.07	14.02	18.12	0.16	0.19	b.d.	b.d.	b.d.	0.05	99.94	73.2	20.7
	14YP-12-9-1	21.74	44.42	0.05	15.04	17.23	0.16	0.20	b.d.	b.d.	0.02	0.89	99.75	71.6	24.7
	14YP-12-9-14	22.29	43.17	b.d.	16.01	16.16	0.18	0.25	b.d.	0.01	b.d.	1.08	99.14	68.4	25.7

b.d. = below detection limit,  $\text{FeO}^t$  = total iron oxide, Mg# =  $100 \times \text{Mg}/(\text{Mg} + \text{Fe}^{2+})$ , Cr# =  $100 \times \text{Cr}/(\text{Cr} + \text{Al})$

Lian et al. (2016), HREE contents suggest that the Gongzhu peridotite have experienced ~10% partial melting. In the Gongzhu peridotite, LREE contents are distinctively enriched, which is inconsistent with the result of partial melting. These U- or spoon-shaped chondrite-normalized REE patterns suggest that the Gongzhu peridotites are not only simply mantle melting relicts, but also may have been refertilized.

#### Implications from platinum-group elements (PGEs)

PGE contents in peridotites are mainly controlled by both partial melting and melt-rock reaction processes. As shown in Fig. 11a, The Gongzhu and Dajiweng peridotites have quite different primitive mantle-normalized PGE patterns (Fig. 11a). Many studies have been carried out on the distribution of PGE in the constituent minerals of mantle peridotites (Mitchell and Keays 1981; Auge 1985; Pattou et al. 1996; Alard et al. 2000). Mitchell and Keays (1981) determined the distribution of PGE in the rock-forming minerals of spinel- and garnet- peridotite xenoliths. Proceeding from garnet, olivine, orthopyroxene, clinopyroxene to spinel, increasing PGE contents have been identified (Mitchell and Keays 1981). However, whole rock PGE contents calculated from modal mineralogy are lower than those actually determined by a radiochemical neutron activation method indicating that 60–80% of bulk PGE exists in sulphide-rich components (Mitchell and Keays 1981). Later in situ proton microscope studies of sulphides (Bulanova et al. 1996; Guo et al. 1999) and analyses of separated sulphide fractions (Hart and Ravizza 1996; Pattou et al. 1996) confirmed sulphide to be the main host phases for PGE in the mantle peridotites. Sulphides in

peridotites occur mainly as inclusions in silicate grains or as inter-granular phases. Alard et al. (2000) used laser ablation inductively coupled plasma mass spectrometry to study the contents of PGEs and Au in these two different sulphides. The results showed that sulphide inclusions generally have higher Os and Ir contents but lower Pd/Os ratios, whereas interstitial sulphides have lower Os and Ir contents and higher Pd/Os ratios (Fig. 11b) (Alard et al. 2000). IPGE may also occur as discrete minerals such as Ru-Os-Ir alloys (Brenan and Andrews 2001; Andrews and Brenan 2002). In Fig. 11a, clear platinum enrichment relative to primitive mantle can be observed. Alard et al. (2000) found that there is no mass balance between whole-rock Pt abundances and average sulphide contents in peridotites, suggesting that a certain amount of Pt either enters other minor sulphide phases or occurs as discrete minerals such as Pt alloys. These Pt-hosting phases may be retained in the mantle residues, resulting in higher Pt contents during melting processes. In the primitive mantle-normalized diagrams, the PGE patterns of the Gongzhu peridotites exhibit Os enrichment and distinct Pd depletion similar to those of sulphide inclusions, and the PGE patterns of the Dajiweng peridotites are consistent with those of interstitial sulphides (Fig. 11a).

During mantle melting, interstitial sulphides are very easily consumed, while alloys and sulphide inclusions are preserved in the melting residues. As such, the melting residues will have higher Os, but lower Pd contents relative to those of primitive mantle. Most interstitial sulphides should have been consumed for the Dajiweng peridotites after such high degree of partial melting, and thus the Dajiweng peridotites should have low PPGE

**Table 5** Whole-rock major and trace element compositions of the Gongzhu peridotites

Sample	14YP-12-4	14YP-12-5	14YP-12-6	14YP-12-7	14YP-12-8	14YP-12-9	14YP-13-4	14YP-13-6	14YP-13-6R	GDW07105 Meas.	GDW07105 Rec.
Major oxides (wt.%)											
SiO <sub>2</sub>	40.34	40.86	40.88	40.6	41.55	40.45	40.67	41.89	41.76	44.48	44.64
	1.68	1.53	1.59	1.32	1.73	1.24	1.8	1.73	1.72	13.84	13.83
Al <sub>2</sub> O <sub>3</sub>											
CaO	1.81	1.67	1.7	1.35	1.67	1.28	1.86	1.37	1.36	8.84	8.81
	2.38	2.72	2.84	2.94	2.55	3.04	2.67	3.67	3.54	5.11	n.m.
Fe <sub>2</sub> O <sub>3</sub>											
FeO	5.07	5.07	4.85	5.1	5.17	4.96	5.17	4.06	n.m.	n.m.	n.m.
K <sub>2</sub> O	0.02	0.02	0.02	0.02	0.02	0.02	0.02	0.02	0.02	2.3	2.32
MgO	38.46	39.21	38.65	39.81	38.95	39.6	38.13	36.94	36.84	7.79	7.77
MnO	0.11	0.12	0.12	0.12	0.12	0.12	0.12	0.12	0.12	0.17	n.m.
	0.38	0.39	0.39	0.39	0.39	0.39	0.4	0.4	0.37	3.39	3.38
Na <sub>2</sub> O											
P <sub>2</sub> O <sub>5</sub>	b.d.	0.01	0.01	b.d.	b.d.	b.d.	b.d.	0.02	0.02	0.94	n.m.
TiO <sub>2</sub>	0.03	0.04	0.04	0.03	0.03	0.02	0.03	0.03	0.03	2.36	n.m.
CO <sub>2</sub>	0.51	0.31	0.39	0.31	0.31	0.26	0.41	0.39	n.m.	n.m.	n.m.
	8.72	7.58	8.42	7.68	7.1	8.14	8.5	9.1	n.m.	n.m.	n.m.
H <sub>2</sub> O+											
LOI	8.7	7.49	8.19	7.43	6.78	7.82	8.35	9.06	n.m.	n.m.	n.m.
S	0.023	0.019	0.018	0.014	0.014	0.013	0.016	0.015	n.m.	n.m.	n.m.
Total	99.51	99.53	99.90	99.67	99.59	99.52	99.78	99.74			
Trace elements (ppm)											
Li	2.31	1.80	1.90	1.92	1.77	1.65	1.78	3.26	n.m.	9.86	9.5
Sc	12.2	11.8	11.8	11.3	12.1	10.6	12.5	11.4	n.m.	16.7	15.2
Ti	122	194	207	104	138	87	149	130	n.m.	15,535	14,200
V	50.8	47.7	50.2	44.4	51.8	39.3	54.9	49.0	n.m.	171	167
Cr	2278	2412	2490	2244	2429	2016	2175	2440	n.m.	149	134
Co	97.4	100.3	100.3	102.5	100.8	97.1	95.6	95.3	n.m.	49.8	46.5
Ni	1704	1761	1788	1797	1740	1715	1721	1667	n.m.	146	140
Cu	16.1	17.5	21.8	8.2	15.6	6.8	23.9	18.8	n.m.	48.4	49
Zn	42.0	44.0	46.8	50.9	44.7	43.8	43.6	45.8	n.m.	197	150
Ga	1.34	1.33	1.43	1.30	1.51	1.26	1.53	1.56	n.m.	26	24.8
Rb	0.27	0.16	0.23	0.23	0.23	0.27	0.24	0.30	n.m.	40.7	37
Ba	1.20	1.74	1.65	1.30	1.79	2.33	1.07	4.29	n.m.	546	527
Th	0.009	0.015	0.017	0.017	0.021	0.032	0.012	0.020	n.m.	6.2	6
U	0.19	0.17	0.19	0.24	0.18	0.25	0.32	0.23	n.m.	1.51	1.4
Nb	0.335	0.368	0.357	0.382	0.392	0.351	0.342	0.295	n.m.	79.5	68
Ta	0.008	0.008	0.007	0.009	0.009	0.008	0.006	0.006	n.m.	4.07	4.3
La	0.070	0.324	0.085	0.078	0.230	0.101	0.076	0.105	n.m.	55	56
Ce	0.114	0.555	0.146	0.144	0.369	0.177	0.136	0.185	n.m.	106	105
Pr	0.015	0.050	0.016	0.018	0.040	0.020	0.015	0.022	n.m.	12.2	13.2
Sr	0.698	1.101	0.921	0.919	1.171	1.900	0.689	2.188	n.m.	1202	1100
Nd	0.074	0.168	0.067	0.085	0.153	0.079	0.063	0.077	n.m.	50.6	54
Zr	0.129	0.148	0.355	0.513	0.871	0.197	0.181	0.219	n.m.	318	277
Hf	0.010	0.016	0.019	0.016	0.041	0.012	0.018	0.019	n.m.	6.82	6.5
Sm	0.022	0.036	0.025	0.022	0.039	0.025	0.028	0.035	n.m.	10.6	10.2

**Table 5** (continued)

Sample	14YP-12-4	14YP-12-5	14YP-12-6	14YP-12-7	14YP-12-8	14YP-12-9	14YP-13-4	14YP-13-6	14YP-13-6R	GDW07105 Meas.	GDW07105 Rec.
Eu	0.012	0.009	0.008	0.009	0.007	0.009	0.010	0.010	n.m.	3.27	3.2
Gd	0.064	0.045	0.048	0.042	0.076	0.033	0.073	0.041	n.m.	9.53	8.5
Tb	0.016	0.011	0.008	0.007	0.017	0.009	0.016	0.013	n.m.	1.23	1.2
Dy	0.127	0.071	0.077	0.066	0.141	0.058	0.128	0.104	n.m.	5.84	5.6
Y	0.885	0.576	0.645	0.480	0.861	0.440	0.923	0.699	n.m.	23.7	22
Ho	0.034	0.022	0.023	0.017	0.034	0.015	0.036	0.026	n.m.	0.9	0.88
Er	0.120	0.079	0.081	0.051	0.114	0.052	0.118	0.081	n.m.	2.24	2
Tm	0.021	0.014	0.013	0.011	0.018	0.010	0.022	0.014	n.m.	0.23	0.28
Yb	0.134	0.091	0.098	0.070	0.135	0.074	0.133	0.122	n.m.	1.29	1.50
Lu	0.020	0.014	0.018	0.016	0.025	0.011	0.023	0.024	n.m.	0.17	0.19
PGE (ppb)											
Pt	4.80	5.79	6.41	4.93	3.97	5.05	4.91	5.43	6.69	n.m.	n.m.
Pd	4.31	5.30	5.49	5.05	3.75	4.64	4.55	4.36	5.73	n.m.	n.m.
Rh	0.74	0.94	0.98	0.81	0.71	0.87	0.80	0.82	1.16	n.m.	n.m.
Ru	4.23	5.19	4.88	4.70	3.69	4.86	4.59	4.53	5.05	n.m.	n.m.
Ir	2.31	2.71	2.90	2.47	2.17	2.54	2.48	2.56	3.2	n.m.	n.m.
Os	3.82	4.36	4.04	5.69	3.00	4.31	4.23	4.00	4.78	n.m.	n.m.

b.d. = below detection limit, n.m. = not measured

contents (Lian et al. 2016). However, the Dajiweng peridotites show clear Pd enrichments instead, suggesting that these peridotites are not simply melting residues and that extra sulphides may have been added into the peridotites during melt-rock reaction (Lian et al. 2016). Although relative IPGE enrichment is observed in the Gongzhu peridotites, no Pd enrichment exists indicating that no or

little Pd-enriched sulphides have precipitated during melt-rock reaction.

To better constrain the behavior of PGEs and also chalcophile elements such as Cu and S, we have plotted PGEs, Cu and  $\text{Al}_2\text{O}_3$  against S for both the Gongzhu peridotites in Fig. 12. Data of the Luobusa peridotites (Yang et al. unpublished, available if required) are also plotted in the same diagrams to better demonstrate the behavior of these elements.  $\text{Al}_2\text{O}_3$  is incompatible during mantle melting and relatively conservative with respect to secondary magmatic processes, making it an effective indicator of the degree of depletion. In Fig. 12h,  $\text{Al}_2\text{O}_3$  and S show a linear correlation, indicating that S contents in the Gongzhu peridotites are controlled mainly by mantle melting process. The negative correlation between IPGE and S and the positive correlation between PPGE and S are consistent with the different compatibilities of these elements during mantle melting (Fig. 12).

In summary, the Gongzhu peridotites have distinctly different PGE characteristics from those of the Dajiweng peridotites. The Dajiweng peridotites have been interpreted as having formed in a forearc tectonic setting and subsequently modified by boninitic melt from the mantle wedge above a suprasubduction zone (Lian et al. 2016). The different PGE features of the Gongzhu peridotites indicate that the Gongzhu peridotites have experienced no melt/fluid-rock reaction processes or been modified by a melt different to that of the Dajiweng peridotites.

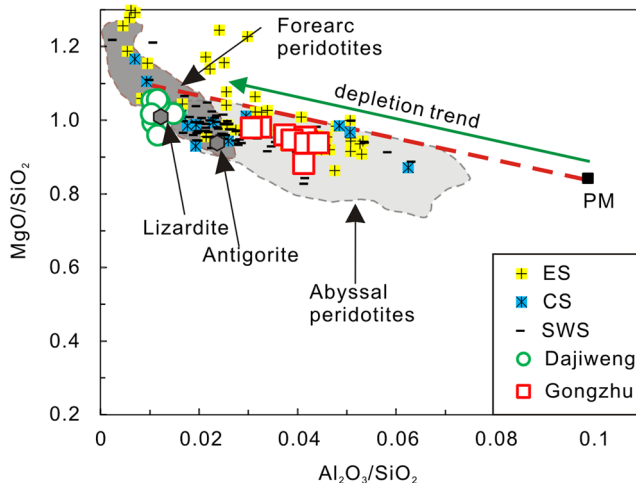
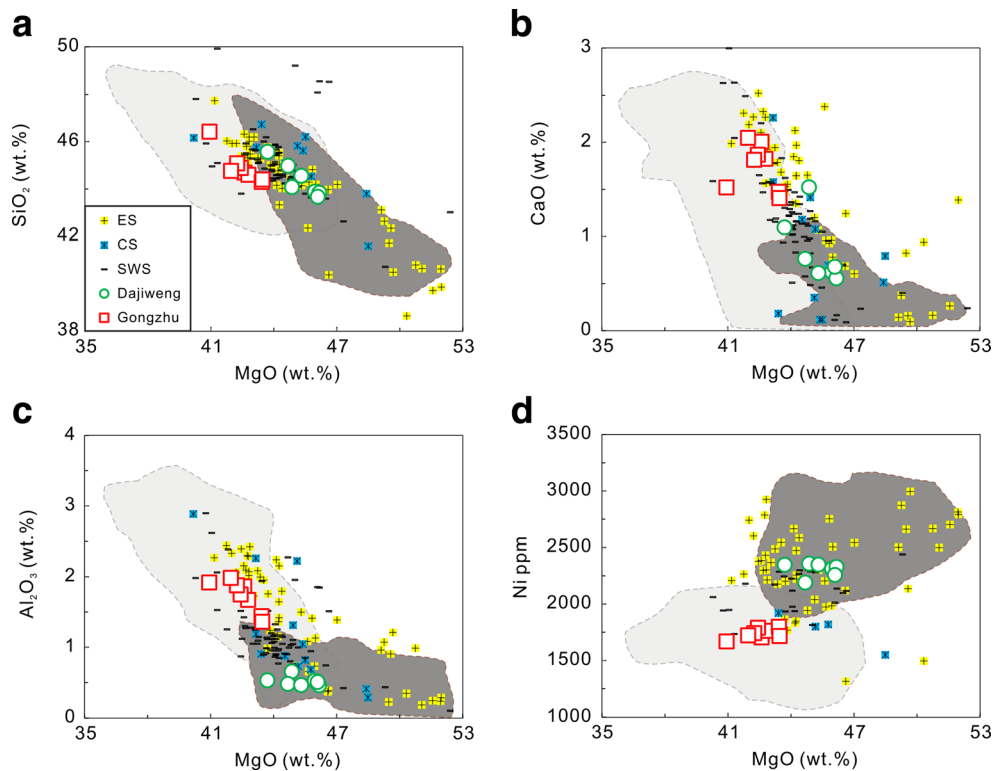


**Fig. 8** Whole-rock MgO and  $\text{Al}_2\text{O}_3$  contents normalized to  $\text{SiO}_2$  contents of peridotites from the YSZS. The peridotite depletion trend is from Snow and Dick (1995). Primitive mantle values are from McDonough and Sun (1995). Abyssal peridotites data are from Niu et al. (1997), and forearc peridotites data are from Parkinson and Pearce (1998) and Ishii (1992)

**Fig. 9** Whole-rock SiO<sub>2</sub> **a**, CaO **b**, Al<sub>2</sub>O<sub>3</sub> **c** and Ni **d** against MgO of peridotites from the YZSZ



### Mantle metasomatism

LREE are more incompatible than HREE, thus, mantle peridotites that underwent partial melting should show LREE-depleted patterns in the primitive-mantle normalized diagram. LREE-enriched characteristics are both common in SSZ type and abyssal peridotites (Lian et al. 2016), and have been interpreted as the result of mantle metasomatism (Parkinson and Pearce 1998; Bizimis et al. 2000; Pearce et al. 2000; Niu 2004). Both the Gongzhu and Dajiweng peridotites exhibit LREE-enriched patterns, which are inconsistent

with the modeled results of simple partial melting (Fig. 10a). Thus, the LREE-enriched characteristics suggest that these peridotites have been metasomatized by LREE-enriched melts/fluids.

PGE characteristics of mantle peridotites can also provide important information on the chemical features of metasomatic melts. Due to the extremely high partition coefficients between sulphide melts and silicate melts (Peach et al. 1994), the PGE contents of melts strongly depend on the state of sulphur (S) saturation (Hamlyn et al. 1985). Primary mid-ocean ridge basalt (MORB) magmas generated by low degree partial

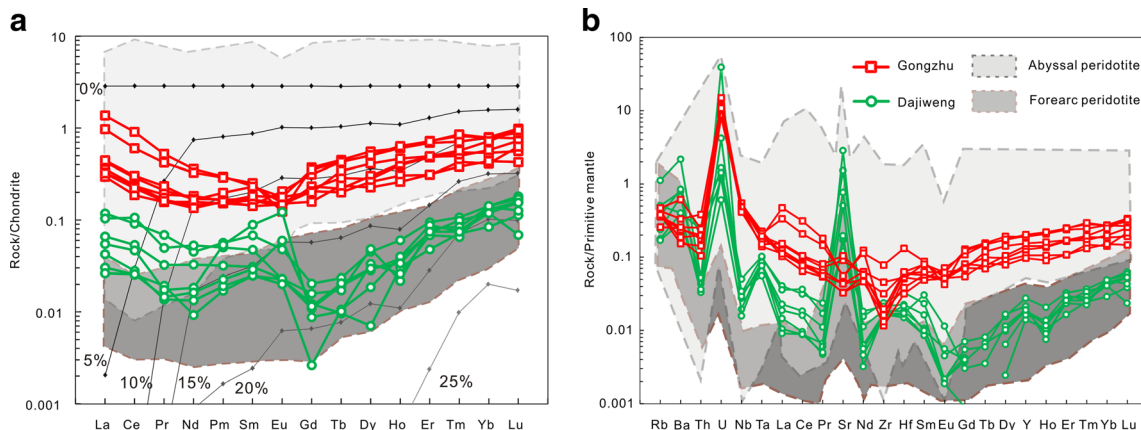


**Fig. 10** **a** Chondrite-normalized REE patterns for the Gongzhu peridotites; **b** Primitive mantle-normalized trace element spider diagram. The Dajiweng peridotites are also shown for comparison. Abyssal peridotites data are from Niu et al. (1997). Forearc peridotites data are

from Parkinson and Pearce (1998). Chondrite values are from Sun and McDonough (1989) and primitive mantle values are from McDonough and Sun (1995)

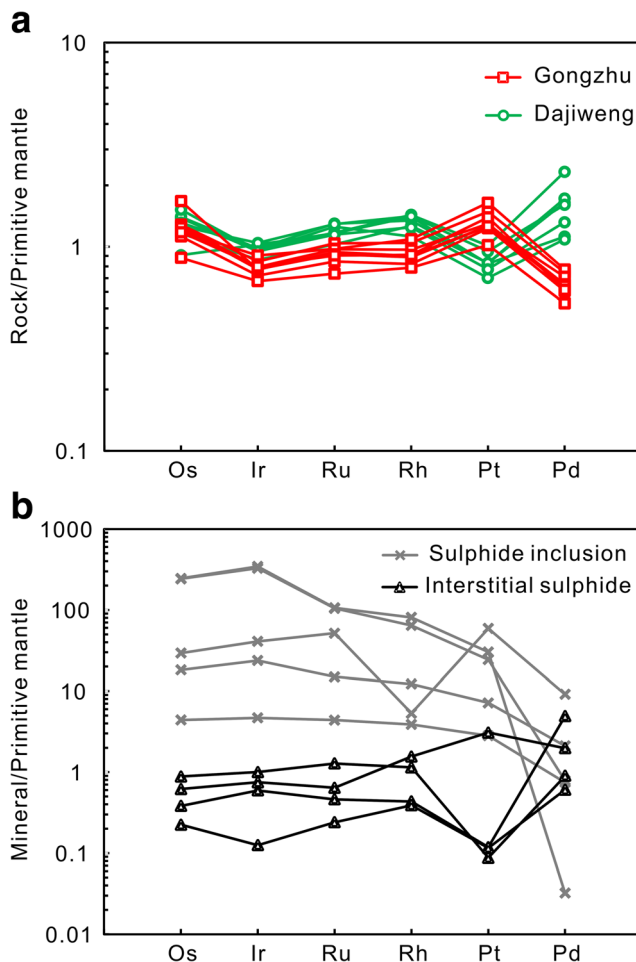


**Fig. 11** a Primitive mantle-normalized PGE patterns for the Gongzhu peridotites. (A) Primitive mantle-normalized PGE patterns for different types of sulphides. The Dajiweng peridotites are also shown for comparison. PGEs contents of sulphide inclusions and interstitial sulphides are from Alard et al. (2000). Primitive mantle values are from McDonough and Sun (1995)

melting of primitive mantle are S-saturated and consequently leave behind PGE-enriched sulphides in residual peridotites (Mitchell and Keays 1981; Hamlyn et al. 1985; Lorand et al. 1993) and thus the melts will become PPGE-depleted. However, boninitic magmas generated by remelting of depleted residual peridotites are strongly S-unsaturated and PGE-enriched (Mitchell and Keays 1981; Hamlyn et al. 1985; Zhou et al. 1998; Woodland et al. 2002). According to the quite low HREE contents and the mineral chemistry, the LREE- and PPGE-enrichments in the Dajiweng peridotites have been interpreted to be metasomatized by boninitic melts in the mantle wedge above the subduction zone (Lian et al. 2016). Considering the low PGE contents of the S-saturated MORB-type melts, reaction of the peridotites with these melts, might not change the PGE patterns of the peridotites in a significant way. However, the LREE-depleted characteristic of these MORB-type melts suggest that they are not the potential melts that have reacted with the Gongzhu peridotites.

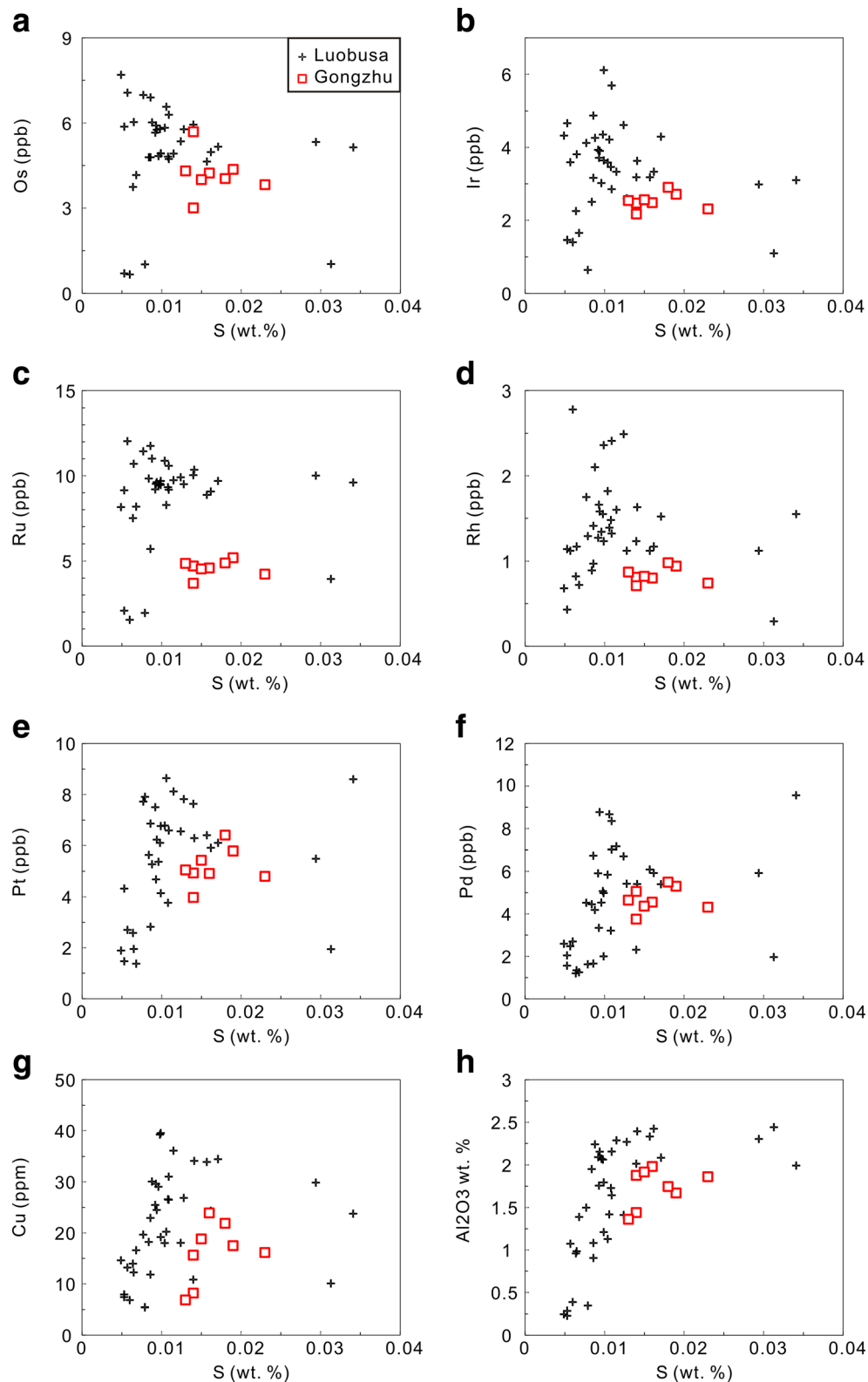
No Pd enrichments were observed in the Gongzhu peridotites, which also excludes the possibility of the boninitic melts being the potential reacting fluid/melt. According to the REE and PGE patterns, we concluded that the Gongzhu peridotites may have been modified by a LREE-enriched fluid without significantly changing the PGE patterns.

### Tectonic setting

Mineral and whole rock geochemical characteristics of peridotites are very sensitive to tectonic setting and can thus be used to reveal the environment of formation of peridotites (Dick and Bullen 1984; Pearce et al. 1984; Pearce 2008). Lian et al. (2016) summarized the mineral and whole-rock chemistry of forearc, back-arc and abyssal peridotites. In the geochemical diagrams of mineral and whole-rock compositions, back-arc peridotites always fall within the field of abyssal peridotites, and thus peridotites chemically consistent with abyssal peridotites may also form in the back-arc basin of the subduction zone. In the  $\text{Al}_2\text{O}_3$  and  $\text{Cr}_2\text{O}_3$  vs. Mg# plots for both Opx and Cpx (Fig. 6), the Gongzhu peridotites plot within the field of abyssal peridotites, whereas the Dajiweng peridotites fall in the field of fore-arc peridotites (Lian et al. 2016). In the Cr# (spinel) vs. Mg# (olivine) and Mg# (spinel) diagrams, the Gongzhu peridotites also cluster in the abyssal peridotite field (Fig. 7).

Major element oxides of the Gongzhu peridotites show affinities to abyssal peridotites with low MgO and Ni contents but high  $\text{Al}_2\text{O}_3$  and CaO contents. In the chondrite-normalized REE diagrams, the Gongzhu peridotites are similar to abyssal peridotites but different from the depleted forearc peridotites from the Izu-Bonin-Mariana arc (Ishii 1992; Parkinson and Pearce 1998; Niu 2004). The Dajiweng peridotites have been interpreted as having been modified by melts from a suprasubduction zone setting (Lian et al. 2016). Based on the mineral and whole-rock geochemical data, the less-depleted Gongzhu peridotites are consistent with abyssal peridotites. As these less-depleted peridotites have been recovered in both the back-arc (Ohara et al. 2002; Ohara et al. 2003) and mid-ocean ridge (Ross and Elthon 1997; Seyler et al. 2003; Brunelli et al. 2006) of the modern ocean, the tectonic setting of the Gongzhu peridotites might be either a back-arc in the subduction zone or a mid-ocean ridge environment. Mafic rocks intruding the Cuobuzha, Jianabeng and Baer massifs in the northern branch of the Western YSZS show affinities to the forearc basin basalt (FABB) (Reagan et al. 2010) or the back-arc basin basalt (BABB) (Pearce et al. 2005; Pearce 2014), indicating the addition of subduction components during the formation of these magmatic rocks (Liu et al. 2015b). Thus, the more plausible tectonic setting for the Gongzhu peridotites should be subduction-related back-arc setting rather than a subduction-unrelated mid-ocean ridge setting.

**Fig. 12** Whole-rock Os **a**, Ir **b**, Ru **c**, Rh **d**, Pt **e**, Pd **f**, Cu **g** and  $\text{Al}_2\text{O}_3$  **h** against S of the Gongzhu peridotites. The Luobusa peridotites (Yang et al. unpublished) are also plotted to better show the relationship between different elements



Peridotites along the YZSZ have been extensively studied. Here, we summarize the published mineral and whole rock chemistry data of peridotites to provide better understanding of the Gongzhu peridotites. In order to simplify the mineral

and whole-rock chemical diagram, we have classified these ophiolites into three groups, the eastern segment (ES), central segment (CS) and western segment (WS), following the traditional subdivision of the Yarlung Zangbo ophiolitic belt.

The eastern segment includes the Luobusa and Kangjinla ophiolites (Malpas et al. 2003; Xu et al. 2011). The central segment includes the Xigaze (Dubois-Cote et al. 2005; Guilmette et al. 2009) and Sangsang ophiolites (Bédard et al. 2009). From Saga to the west, the western segment of YZSZ ophiolitic belt comprises two branches. The southern branch of the western segment (SWS) includes the Saga (Bédard et al. 2009), Zhongba (Dai et al. 2011), Xiugugabu (Bezard et al. 2011), Purang (also called Yungbwa or Jungbwa) (Liu et al. 2010) and Dongbo (also called Kiogar) ophiolite (Liu et al. 2015a; Niu et al. 2015). As shown in Figs. 5, 6, and 7, mineral and whole-rock geochemical compositions of these three segments all show an evolutionary trend from abyssal (low melting degree) to forearc peridotites (high melting degree). Mafic rocks in the YZSZ show compositions ranging from N-MORB to IAT-CAB and to OIB end-members (Hébert et al. 2012). Two different models have been proposed for the origin of the ophiolitic peridotites in the YZSZ, including (1) two-stage evolution model (Dubois-Cote et al. 2005; Zhou et al. 2005; Liu et al. 2010; Xu et al. 2011). In this model, peridotites were first suggested to form in a mid-ocean ridge environment and then be trapped and modified in a SSZ environment; (2) an intra-oceanic forearc-arc-back arc system in a subduction zone setting (Aitchison et al. 2000; Hébert et al. 2003; Guilmette et al. 2009). Lian et al. (2016) also proposed that peridotites in the western segment of the YZSZ formed in the intra-oceanic subduction system, which suggests that the Gongzhu peridotites may have formed in the back-arc basin of the intra-oceanic subduction zone.

Subduction-initiation has been suggested to play an important role in the formation of most ophiolites (Stern 2004; Wakabayashi et al. 2010; Whattam and Stern 2011; Stern et al. 2012; Zhang et al. 2016). Whattam and Stern (2011) classified ophiolites into the SIR and non-SIR ophiolites. SIR ophiolites are those which follow the ‘subduction initiation rule (SIR)’ (Whattam and Stern 2011). Compositions of magmatic rocks in the SIR ophiolites generally show from less to more HFSE-depleted and LILE-enriched variations, and correspondingly, the peridotites evolved from less to more depleted compositions (Whattam and Stern. 2011). As summarized by Liu et al. (2015b), mafic dikes in the western segment of the YZSZ show a clear trend from the N-MORB to island arc basalt, which is consistent with the magmatic trend of SIR ophiolites. It then follows that another plausible explanation for the tectonic setting of the Gongzhu peridotite is that both the Dajiweng and Gongzhu peridotites represent two end-members of the SIR ophiolite and both formed in the same incipient forearc/proto-forearc stage of the intra-oceanic subduction. As depicted by Whattam and Stern (2011), peridotites in the western YZSZ may have formed in the following steps: (1) the sinking of the

subduction slab results in the upwelling of the asthenosphere; (2) decompression melting of the upwelling asthenospheric mantle source generated the FAB-type magmas observed in the western YZSZ and depleted mantle peridotites (e.g. the Gongzhu peridotites) formed at this stage; (3) peridotites such as the Dajiweng peridotites formed due to the hydrous melting of the already depleted mantle and were modified by the boninitic melts in the suprasubduction zone.

We propose two possible tectonic settings of the Gongzhu peridotites, namely (1) the Gongzhu peridotites formed in the back-arc setting of an intra-oceanic subduction system and (2) the Gongzhu and Dajiweng peridotites both formed in the in the same incipient forearc/proto-forearc environment of an intra-oceanic subduction zone.

## Conclusions

The Gongzhu massif is dominated by peridotites with minor gabbros, volcanic rocks and cherts. The peridotites consist of lherzolites with modal clinopyroxene contents ranging from 6%–7%. Mg# values of silicate minerals are relatively low compared to the Dajiweng peridotite in the same belt. The Cr# values of spinels from the Gongzhu peridotite range from 18 to 26 with an estimated degree of melting varying from 7% to 10%. Chondrite-normalized REE patterns of the Gongzhu peridotite have LREE-enriched characteristics. No, or very small PPGE enrichment has been observed in the Gongzhu peridotites. Combining the REE and PGE characteristics, the Gongzhu peridotites have been modified by LREE-enriched fluids in a subduction zone setting. Based on the petrological, mineralogical and geochemical studies, we propose that the Gongzhu peridotites formed either in the back-arc setting of an intra-oceanic subduction system or that the Gongzhu and Dajiweng peridotites both formed in the same incipient forearc/proto-forearc environment of an intra-oceanic subduction zone.

**Acknowledgements** We thank He Rong for the assistance with the microprobe analyses and the China National Research Center for the geochemical analyses. We would also like to thank Michael Wiedenbeck, Alexander Rocholl, Pengfei Zhang, Ziliang Jin, Cong Zhang, Paul T. Robinson and Julian A. Pearce for their valuable suggestions in modifying this manuscript. Two reviewers and the editors are greatly appreciated for their critical and constructive comments and suggestions which greatly improved the manuscript. This research was funded by grants from the China Scholarship Council, the Ministry of Science and Technology of China (2014DFR21270), China Geological Survey (121201102000150069, 12120115027201, DD20160023-01, and 201511022), the International Geoscience Programme (IGCP-649) and the Fund from the State Key Laboratory of Continental Tectonics and Dynamics (Z1301-a20) and (Z1301-a22).

## References

- Aitchison JC, Davis AM, Liu J, Luo H, Malpas JG, McDermid IR, Wu H, Ziabrev SV, Zhou M (2000) Remnants of a cretaceous intra-oceanic subduction system within the Yarlung–Zangbo suture (southern Tibet). *Earth Planet Sc Lett* 183:231–244
- Alard O, Griffin WL, Lorand JP, Jackson SE, O'Reilly SY (2000) Non-chondritic distribution of the highly siderophile elements in mantle sulphides. *Nature* 407:891–894
- Andrews DR, Brenan JM (2002) Phase-equilibrium constraints on the magmatic origin of laurite + Ru–Os–Ir alloy. *Can Mineral* 40: 1705–1716
- Arai S (1994) Characterization of spinel peridotites by olivine–spinel compositional relationships: review and interpretation. *Chem Geol* 113:191–204
- Auge T (1985) Platinum-group-mineral inclusions in ophiolitic chromitite from the Vourinos complex, Greece. *Can Mineral* 23: 163–171
- Baker MB, Stolper EM (1994) Determining the composition of high-pressure mantle melts using diamond aggregates. *Geochim Cosmochim Ac* 58:2811–2827
- Barnes S, Picard CP (1993) The behaviour of platinum-group elements during partial melting, crystal fractionation, and sulphide segregation: an example from the cape smith Fold Belt, northern Quebec. *Geochim Cosmochim Ac* 57:79–87
- Barnes SJ (1993) Partitioning of the platinum group elements and gold between silicate and sulphide magmas in the Munni Munni complex, Western Australia. *Geochim Cosmochim Ac* 57:1277–1290
- Bédard É, Hébert R, Guilmette C, Lesage G, Wang CS, Dostal J (2009) Petrology and geochemistry of the Saga and Sangsang ophiolitic massifs, Yarlung Zangbo suture zone, southern Tibet: evidence for an arc-back-arc origin. *Lithos* 113:48–67
- Bezard R, Hébert R, Wang C, Dostal J, Dai J, Zhong H (2011) Petrology and geochemistry of the Xiugugabu ophiolitic massif, western Yarlung Zangbo suture zone, Tibet. *Lithos* 125:347–367
- Bizimis M, Salters VJ, Bonatti E (2000) Trace and REE content of clinopyroxenes from supra-subduction zone peridotites. Implications for melting and enrichment processes in island arcs. *Chem Geol* 165:67–85
- Brenan JM, Andrews D (2001) High-temperature stability of laurite and Ru–Os–Ir alloy and their role in PGE fractionation in mafic magmas. *Can Mineral* 39:341–360
- Brunelli D, Seyler M, Cipriani A, Ottolini L, Bonatti E (2006) Discontinuous melt extraction and weak refertilization of mantle peridotites at the Vema lithospheric section (mid-Atlantic ridge). *J Petrol* 47:745–771
- Bulanova GP, Griffin WL, Ryan CG, Shestakova OY, Barnes S (1996) Trace elements in sulfide inclusions from Yakutian diamonds. *Contrib Mineral Petrol* 124:111–125
- Burg JP, Chen GM (1984) Tectonics and structural zonation of southern Tibet. *China Nature*:219–223
- Dai J, Wang C, Hébert R, Santosh M, Li Y, Xu J (2011) Petrology and geochemistry of peridotites in the Zhongba ophiolite, Yarlung Zangbo suture zone: implications for the early cretaceous intra-oceanic subduction zone within the neo-Tethys. *Chem Geol* 2011: 133–148
- Dick HJB, Bullen T (1984) Chromian spinel as a petrogenetic indicator in abyssal and alpine-type peridotites and spatially associated lavas. *Contrib Mineral Petrol* 86:54–76
- Dilek Y, Furnes H (2011) Ophiolite genesis and global tectonics: geochemical and tectonic fingerprinting of ancient oceanic lithosphere. *Geol Soc Am Bull* 123:387–411
- Dilek Y, Furnes H (2014) Ophiolites and their origins. *Elements* 10:93–100
- Ding L, Kapp P, Wan X (2005) Paleocene–Eocene record of ophiolite obduction and initial India-Asia collision, south Central Tibet. *Tectonics* 24
- Dubois-Cote V, Hebert R, Dupuis C, Wang CS, Li YL, Dostal J (2005) Petrological and geochemical evidence for the origin of the Yarlung Zangbo ophiolites, southern Tibet. *Chem Geol* 214:265–286
- Girardeau J, Mercier J, Yougong Z (1985) Structure of the Xigaze ophiolite, Yarlung Zangbo suture zone, southern Tibet, China: genetic implications. *Tectonics* 4:267–288
- Guilmette C, Hébert R, Wang C, Villeneuve M (2009) Geochemistry and geochronology of the metamorphic sole underlying the Xigaze ophiolite, Yarlung Zangbo suture zone, South Tibet. *Lithos* 112: 149–162
- Guo J, Griffin WL, O'Reilly SY (1999) Geochemistry and origin of sulphide minerals in mantle xenoliths: Qilin, southeastern China. *J Petro* 40:1125–1149
- Hamlyn PR, Keays RR, Cameron WE, Crawford AJ, Waldron HM (1985) Precious metals in magnesian low-Ti lavas: implications for metallogenesis and sulfur saturation in primary magmas. *Geochim Cosmochim Ac* 49:1797–1811
- Hart SR, Ravizza GE (1996) Os partitioning between phases in lherzolite and basalt. *Geophysical Monograph-American Geophysical Union* 95:123–134
- Hébert R, Bezard R, Guilmette C, Dostal J, Wang CS, Liu ZF (2012) The Indus–Yarlung Zangbo ophiolites from Nanga Parbat to Namche Barwa syntaxes, southern Tibet: first synthesis of petrology, geochemistry, and geochronology with incidences on geodynamic reconstructions of neo-Tethys. *Gondwana Res* 22:377–397
- Hébert R, Huot F, Wang C, Liu Z (2003) Yarlung Zangbo ophiolites (southern Tibet) revisited: geodynamic implications from the mineral record. *Geol Soc Lond, Spec Publ* 218:165–190
- Hellebrand E, Snow JE, Dick HJ, Hofmann AW (2001) Coupled major and trace elements as indicators of the extent of melting in mid-ocean-ridge peridotites. *Nature* 410:677–681
- Ishii T (1992) Petrological studies of peridotites from diapiric serpentinite seamounts in the Izu-Ogasawara-Mariana forearc, LEG125 Proc. ODP, Sci. Results. Ocean Drilling Program, College Station, TX, pp 445–485
- Jagoutz E, Palme H, Baddehausen H, Blum K, Cendales M, Dreibus G, Spettel B, Waenke H, Lorenz V (1979) The abundances of major, minor and trace elements in the earth's mantle as derived from primitive ultramafic nodules. *Lunar and Planetary Science Conference Proceedings*, pp 2031–2050
- Jannessary MR, Melcher F, Lodziak J, Meisel TC (2012) Review of platinum-group element distribution and mineralogy in chromitite ores from southern Iran. *Ore Geol Rev* 48:278–305
- Jaques AL, Green DH (1980) Anhydrous melting of peridotite at 0–15 kb pressure and the genesis of tholeiitic basalts. *Contrib Mineral Petrol* 73:287–310
- Klemm W, Bombach G (2001) A simple method of target preparation for the bulk analysis of powder samples by laser ablation inductively coupled plasma mass spectrometry (LA-ICP-MS). *Fresenius J Anal Chem* 370:641–646
- Krishnakanta Singh A (2013) Petrology and geochemistry of abyssal peridotites from the Manipur ophiolite complex, indo-Myanmar Orogenic Belt, Northeast India: implication for melt generation in mid-oceanic ridge environment. *J Asian Earth Sci* 66:258–276
- Lian D, Yang J, Robinson PT, Liu F, Xiong F, Zhang L, Gao J, Wu W (2016) Tectonic evolution of the western Yarlung Zangbo Ophiolitic Belt, Tibet: implications from the petrology, mineralogy, and geochemistry of the peridotites. *J Geo* 124:353–376
- Liang F, Xu Z, Zhao J (2014) In-situ moissanite in dunite: deep mantle origin of mantle peridotite in Luobusa ophiolite, Tibet. *Acta Geologica Sinica (English Edition)* 88:517–529
- Liu CZ, Wu FY, Wilde SA, Yu LJ, Li JL (2010) Anorthitic plagioclase and pargasitic amphibole in mantle peridotites from the Yungbwa

- ophiolite (southwestern Tibetan plateau) formed by hydrous melt metasomatism. *Lithos* 114:413–422
- Liu F, Yang J, Dilek Y, Xu Z, Xu X, Liang F, Chen S, Lian D (2015a) Geochronology and geochemistry of basaltic lavas in the Dongbo and Purang ophiolites of the Yarlung-Zangbo suture zone: plume-influenced continental margin-type oceanic lithosphere in southern Tibet. *Gondwana Res* 27:701–718
- Liu F, Yang J, Lian D, Zhao H, Zhang L (2015b) Genesis and characteristics of the western part of the Yarlung Zangbo ophiolites, Tibet. *Acta Petrol Sin* 31:3609–3628 (in Chinese with an English abstract)
- Lorand J, Pattou L, Gros M (1999) Fractionation of platinum-group elements and gold in the upper mantle: a detailed study in Pyrenean orogenic lherzolites. *J Petrol* 40:957–981
- Lorand JP, Keays RR, Bodinier JL (1993) Copper and noble metal enrichments across the lithosphere—asthenosphere boundary of mantle diapirs: evidence from the Lanzo lherzolite massif. *J Petrol* 34: 1111–1140
- Malpas J, Zhou M, Robinson PT, Reynolds PH (2003) Geochemical and geochronological constraints on the origin and emplacement of the Yarlung Zangbo ophiolites, southern Tibet. *Geol Soc Lond, Spec Publ* 218:191–206
- McDonough WF, Sun S (1995) The composition of the Earth. *Chem Geol* 120:223–253
- Melcher F, Meisel T, Puhl J, Koller F (2002) Petrogenesis and geotectonic setting of ultramafic rocks in the eastern alps: constraints from geochemistry. *Lithos* 65:69–112
- Mitchell RH, Keays RR (1981) Abundance and distribution of gold, palladium and iridium in some spinel and garnet lherzolites: implications for the nature and origin of precious metal-rich intergranular components in the upper mantle. *Geochim Cosmochim Ac* 45: 2425–2442
- Nicolas A, Girardeau J, Marcoux J, Dupré B, Xibin W, Yougong C, Haixiang Z, Xuchang X (1981) The Xigaze ophiolite (Tibet): a peculiar oceanic lithosphere. *Nature*:414–417
- Niu Y (1997) Mantle melting and melt extraction processes beneath ocean ridges: evidence from abyssal peridotites. *J Petrol* 38:1047–1074
- Niu X, Yang J, Dilek Y, Xu J, Li J, Chen S, Feng G, Liu F, Xiong F, Liu Z (2015) Petrological and Os isotopic constraints on the origin of the Dongbo peridotite massif, Yarlung Zangbo suture zone, western Tibet. *J Asian Earth Sci* 110:72–84
- Niu Y (2004) Bulk-rock major and trace element compositions of abyssal peridotites: implications for mantle melting, melt extraction and post-melting processes beneath mid-ocean ridges. *J Petrol* 45: 2423–2458
- Ohara Y, Fujioka K, Ishii T, Yurimoto H (2003) Peridotites and gabbros from the Parece vela backarc basin: unique tectonic window in an extinct backarc spreading ridge. *Geochim Geophys Geosyst* 4:1–22
- Ohara Y, Stern RJ, Ishii T, Yurimoto H, Yamazaki T (2002) Peridotites from the Mariana trough: first look at the mantle beneath an active back-arc basin. *Contrib Mineral Petrol* 143:1–18
- Osbahr I, Oberthür T, Klemd R, Josties A (2014) Platinum-group element distribution in base-metal sulfides of the UG2 chromitite, bushveld complex, South Africa—a reconnaissance study. *Mineral Deposita* 49:655–665
- Parkinson IJ, Pearce JA (1998) Peridotites from the Izu–Bonin–Mariana forearc (ODP leg 125): evidence for mantle melting and melt–mantle interaction in a supra-subduction zone setting. *J Petrol* 39:1577–1618
- Pattou L, Lorand JP, Gros M (1996) Non-chondritic platinum-group element ratios in the Earth's mantle. *Nature* 379:712–715
- Peach CL, Mathez EA, Keays RR, Reeves SJ (1994) Experimentally determined sulfide melt-silicate melt partition coefficients for iridium and palladium. *Chem Geol* 117:361–377
- Pearce JA (2008) Geochemical fingerprinting of oceanic basalts with applications to ophiolite classification and the search for Archean oceanic crust. *Lithos* 100:14–48
- Pearce JA (2014) Immobile element fingerprinting of ophiolites. *Elements* 10:101–108
- Pearce JA, Barker PF, Edwards SJ, Parkinson IJ, Leat PT (2000) Geochemistry and tectonic significance of peridotites from the south sandwich arc–basin system, South Atlantic. *Contrib Mineral Petrol* 139:36–53
- Pearce JA, Lippard SJ, Roberts S (1984) Characteristics and tectonic significance of supra-subduction zone ophiolites. *Geol Soc Lond, Spec Publ* 16:77–94
- Pearce JA, Parkinson IJ (1993) Trace element models for mantle melting: application to volcanic arc petrogenesis. *Geol Soc Lond, Spec Publ* 76:373–403
- Pearce JA, Stern RJ, Bloomer SH, Fryer P (2005) Geochemical mapping of the Mariana arc–basin system: implications for the nature and distribution of subduction components. *Geochim Geophys Geosyst* 6:1–27
- Penrose CP (1972) Penrose field conference on ophiolites. *Geotimes* 17: 24–25
- Reagan MK, Ishizuka O, Stern RJ, Kelley KA, Ohara Y, Blichert Toft J, Bloomer SH, Cash J, Fryer P, Hanan BB (2010) Fore-arc basalts and subduction initiation in the Izu–Bonin–Mariana system. *Geochim Geophys Geosyst* 11:1–17
- Ross K, Elthon D (1997) Extreme incompatible trace-element depletion of diopside in residual mantle from south of the Kane Fracture Zone Proceedings of the Ocean Drilling Program. Scientific results. Ocean Drilling Program, pp 277–284
- Saka S, Uysal I, Akmaz RM, Kaliwoda M, Hochleitner R (2014) The effects of partial melting, melt–mantle interaction and fractionation on ophiolite generation: constraints from the late cretaceous Pozanti–Karsanti ophiolite, southern Turkey. *Lithos* 2014:300–316
- Seyler M, Cannat M, Mével C (2003) Evidence for major-element heterogeneity in the mantle source of abyssal peridotites from the southwest Indian ridge (52 to 68 E). *Geochim Geophys Geosyst* 4:1–33
- Snow JE, Dick HJ (1995) Pervasive magnesium loss by marine weathering of peridotite. *Geochim Cosmochim Ac* 59:4219–4235
- Stern RJ (2004) Subduction initiation: spontaneous and induced. *Earth Planet Sc Lett* 226:275–292
- Stern RJ, Reagan M, Ishizuka O, Ohara Y, Whattam S (2012) To understand subduction initiation, study forearc crust: to understand forearc crust, study ophiolites. *Lithosphere-US* 4:469–483
- Sun S, McDonough WF (1989) Chemical and isotopic systematics of oceanic basalts: implications for mantle composition and processes. *Geol Soc Lond, Spec Publ* 42:313–345
- Takazawa E, Frey FA, Shimizu N, Obata M (2000) Whole rock compositional variations in an upper mantle peridotite (Horoman, Hokkaido, Japan): are they consistent with a partial melting process? *Geochim Cosmochim Ac* 64:695–716
- Tapponier P, Mercier JL, Proust F, Andrieux J, Armijo R, Bassoulet JP, Brunel M, Burg JP, Colchen M, Dupré B (1981) The Tibetan side of the India–Eurasia collision. *Nature*:405–410
- Uysal İ, Ersoy EY, Karşlı O, Dilek Y, Sadıkclar MB, Ottley CJ, Tiepolo M, Meisel T (2012) Coexistence of abyssal and ultra-depleted SSZ type mantle peridotites in a neo-Tethyan ophiolite in SW Turkey: constraints from mineral composition, whole-rock geochemistry (major–trace–REE–PGE), and Re–Os isotope systematics. *Lithos* 132: 50–69
- Wakabayashi J, Ghatak A, Basu AR (2010) Suprasubduction-zone ophiolite generation, emplacement, and initiation of subduction: a perspective from geochemistry, metamorphism, geochronology, and regional geology. *Geol Soc Am Bull* 122:1548–1568
- Wang C, Li X, Liu Z, Li Y, Jansa L, Dai J, Wei Y (2012) Revision of the cretaceous–Paleogene stratigraphic framework, facies architecture

- and provenance of the Xigaze forearc basin along the Yarlung Zangbo suture zone. *Gondwana Res* 22:415–433
- Whattam SA, Stern RJ (2011) The ‘subduction initiation rule’: a key for linking ophiolites, intra-oceanic forearcs, and subduction initiation. *Contrib Mineral Petrol* 162:1031–1045
- Woodland SJ, Pearson DG, Thirlwall MF (2002) A platinum group element and Re–Os isotope investigation of siderophile element recycling in subduction zones: comparison of Grenada, lesser Antilles arc, and the Izu–Bonin arc. *J Petrol* 43:171–198
- Xiong F, Yang J, Robinson PT, Xu X, Liu Z, Li Y, Li J, Chen S (2015) Origin of podiform chromitite, a new model based on the Luobusa ophiolite, Tibet. *Gondwana Res* 27:525–542
- Xiong FH, Yang JS, Liu Z, Guo GL, Chen SY, Xu XZ, Li Y, Liu F (2013) High-Cr and high-Al chromitite found in western Yarlung-Zangbo suture zone in Tibet. *Acta Petrol Sin* 29:1878–1908 (in Chinese with an English abstract)
- Xu X, Yang J, Ba D, Guo G, Robinson PT, Li J (2011) Petrogenesis of the Kangjinla peridotite in the Luobusa ophiolite, southern Tibet. *J Asian Earth Sci* 42:553–568
- Xu Z, Dilek Y, Yang J, Liang F, Liu F, Ba D, Cai Z, Li G, Dong H, Ji S (2015) Crustal structure of the Indus–Tsangpo suture zone and its ophiolites in southern Tibet. *Gondwana Res* 2015:507–524
- Xu Z, Ji S, Cai Z, Zeng L, Geng Q, Cao H (2012) Kinematics and dynamics of the Namche Barwa Syntaxis, eastern Himalaya: constraints from deformation, fabrics and geochronology. *Gondwana Res* 21:19–36
- Yin A, Harrison TM (2000) Geologic evolution of the Himalayan-Tibetan orogen. *Annu Rev Earth Pl Sc* 28:211–280
- Zhang P, Uysal I, Zhou M, Su B, Avcı E (2016) Subduction initiation for the formation of high-Cr chromitites in the kop ophiolite. NE Turkey. *Lithos*
- Zhou M, Sun M, Keays RR, Kerrich RW (1998) Controls on platinum-group elemental distributions of podiform chromitites: a case study of high-Cr and high-Al chromitites from Chinese orogenic belts. *Geochim Cosmochim Ac* 62:677–688
- Zhou MF, Robinson PT, Malpas J, Edwards SJ, Qi L (2005) REE and PGE geochemical constraints on the formation of dunites in the Luobusa ophiolite, southern Tibet. *J Petrol* 46:615–639
- Zhu D, Zhao Z, Niu Y, Dilek Y, Hou Z, Mo X (2013) The origin and pre-Cenozoic evolution of the Tibetan plateau. *Gondwana Res* 23:1429–1454